Lehmann effect in nematic and cholesteric liquid crystals: a review

P. Oswald, A. Dequidt & G. Poy

View supplementary material

Accepted author version posted online: 29 Sep 2019.
Published online: 17 Oct 2019.

Submit your article to this journal

Article views: 7

View related articles

View Crossmark data

Taylor & Francis
Taylor & Francis Group

REVIEW ARTICLE

Check for updates

Lehmann effect in nematic and cholesteric liquid crystals: a review

P. Oswald[a], A. Dequidt[b] and G. Poy[a]

[a]Univ Lyon, Ens de Lyon, Univ Claude Bernard, CNRS, Laboratoire de Physique, F-69342 Lyon, France; [b]SIGMA Clermont, ICCF, Université Clermont Auvergne, CNRS, Clermont-Ferrand F-63000, France

ABSTRACT
The Lehmann effect is the continuous rotation of cholesteric droplets subjected to a temperature gradient. Discovered by Otto Lehmann in 1900, this effect was re-observed recently by several authors not only in cholesterics but also in nematics when the director field is twisted inside the droplets. In most experiments, the droplets coexist with their isotropic liquid, but the Lehmann effect can also be observed when the droplets are dispersed in an isotropic liquid in which the LC is partly miscible. After a brief history on the Lehmann effect and its first explanation by Leslie in 1968, we will review the main experimental results obtained on this subject from 2008. In particular, the role of the temperature gradient, of the size of the droplets, of the textures and their orientation with respect to the temperature gradient, of the confinement effects, of the impurities and of the concentration of chiral molecules will be described. A special emphasis will also be placed on the research of hydrodynamic effects to answer the fundamental question of whether it is just the texture or the droplet itself that rotates. We will then review the different models proposed in the literature to explain the Lehmann effect. Among them are two thermomechanical models directly based on the Leslie explanation (named TM1 and TM2 models), a thermomechanical model of rotating texture 'surfing' on a heat wave (TM3 model), a model of melting-growth (MG model) that only applies when the droplets coexist with their own isotropic liquid, and a pure hydrodynamic model (H model) based on the existence of Marangoni flows – currently, only evidenced in emulsified cholesterics. The strengths and weaknesses of each model will be discussed in relation with the experimental results.

1. Introduction

Thermomechanical effects are important in materials science. They occur each time a temperature variation produces a force or a stress inside a material. A classical example is the Rayleigh Benard instability in a fluid layer heated from below [1]. In that case, a temperature gradient generates a buoyancy force – the Archimedes force – that destabilizes the layer and produces convection rolls. A thermal gradient can also cause the different parts of a solid to expand by different amounts. This effect generates stresses that may cause the generation and the propagation of cracks inside the solid [2–4]. Another well-known thermomechanical effect is the fountain effect in superfluid helium II. In that case, a temperature gradient inside a tube containing the superfluid generates a pressure gradient responsible for the expulsion of the superfluid out of the tube [5]. Unsteady temperature gradients can also generate flows in expandable liquids even in the absence of gravity [6]. This phenomenon is particularly important in small-scale systems and found applications in microfluidics [7,8]. A similar

phenomenon was observed in nematic liquid crystals (LC) and was found to produce director reorientation [9].

Other thermomechanical effects exist in LCs. Among them is the Lehmann effect discovered in 1900 by Otto Lehmann, a pioneer in the study of LCs [10]. In the Lehmann experiment, cholesteric droplets are set into rotation when they are subjected to a temperature gradient. Although this phenomenon was known for a long time, it has not yet been explained completely. In particular, the origin of the torque responsible for the rotation of the droplets is still under debate, the issue being whether this torque is due to an external flow, or directly due to the heat flux, each molecule acting as a molecular rotor transforming energy from the surrounding environment into rotational motion [11,12]. Not to mention the fact that this effect is perhaps due to an optical illusion, as we will show later within a model of melting-growth. This situation obviously contrasts with that of the previous examples for which the physical origin of the thermomechanical effect is clear.

CONTACT P. Oswald ✉ patrick.oswald@ens-lyon.fr

The goal of this paper is to review the main experimental observations of the Lehmann effect and to discuss the different models proposed so far to explain it. The plan of this review in as follows. Section 2 will be devoted to a brief history on the Lehmann effect and its first explanation given by Leslie in 1968. The main experimental results about the Lehmann effect will be then recalled in Section 3. These experimental results have been obtained more recently, from the 2000s by different groups working mainly in France and in Japan. Finally, we will discuss the different models proposed so far to explain this effect, by focusing on their respective strengths and weaknesses. Finally, our conclusions will be drawn in Section 4.

2. The Lehmann effect and the Leslie explanation: a brief history

The first mention of the Lehmann effect dates from 1900 [10]. In a famous article, Lehmann explains that in samples heated from below, droplets of the liquid crystal p-azoxy phenetole – a nonchiral molecule – rotate constantly anticlockwise when they are dispersed in a mineral oil or in melted sugar. According to Lehmann, this effect could be related to a surface tension effect. However, Lehmann observes that the droplet texture winds up when the temperature gradient increases, as if the droplets were sheared from inside rather than from their surfaces (Figure 1).

Lehmann then multiplied observations with his famous polarizing microscope, which was equipped with a hot stage, and made new crucial findings that were published in his book of 1921 [13]. In this book, Lehmann emphasizes for the first time that the rotation does not occur with every LC. Indeed, a small amount of a chiral impurity which winds the texture in the absence of a temperature gradient must be added to the LC to observe a rotation. In addition, the sense of rotation depends on the chiral molecule. For instance, the droplets rotate clockwise when rosin is added whereas the droplets rotate anticlockwise when cholesteryl benzoate is added. This point is fundamental because it shows for the first time the role of the chirality. Lehmann also notes that the

larger the concentration of chiral impurity, the larger the rotation velocity. Finally, Lehmann observes that the droplets stop rotating (or oscillate, a phenomenon never re-observed to our knowledge) when he adds simultaneously the two impurities in such proportions that their effects on the twist of the texture compensate at zero temperature gradient. On these issues, Lehmann concluded that the rotation only occurs in cholesteric phases, never in nematic phases. We would also add that Lehmann was convinced that it was not the droplet – but its texture – that was rotating because he never observed any flow.

However, the work of Lehmann lacks quantitative information. For instance, the concentrations of chiral molecules, the sample thicknesses, the temperature gradients used experimentally are unknown. In addition, the only movie realized by Lehmann showing the droplet rotation remains missing as we have checked by contacting the production company (UFA-Produktion that still exists) and the Karlsruhe University where Lehmann was working and which has conserved number of archives on him.

From a theoretical point of view, Oseen was the first to propose that, in the Lehmann experiment, the molecules rotated with the same speed around vertical axes drawn through their center of mass [14]. But it was not until 1968 and the work of Leslie on nematodynamics that this issue was raised again and the first explanation was given [15]. In this seminal paper, Leslie proposes new linear constitutive equations between the fluxes and forces. In his theory, the fluxes are the temperature gradient, the velocity gradient and the relative angular velocity of the director. The associated forces are the heat flux and the forces and torques acting on the director. From these equations, Leslie showed that, in a cholesteric phase and for symmetry reasons, the director experiences a torque that is proportional to the temperature gradient. The proportionality coefficient is the Leslie thermomechanical coefficient. In his paper, Leslie proposes that the Lehmann effect is due to this torque. This explanation has become a paradigm which must be revisited in the light of the new experiments presented in the next section.

3. Recent experimental results

It is only from 2008 that controlled experiments on the Lehmann effect have been conducted, first in France and then in Japan. In these experiments, two methods were used to prepare cholesteric and nematic droplets. The first one consisted in heating the LC until its clearing temperature is reached [16]. Because the phase transition is first order, droplets form in the coexistence region between the two phases. The second method consisted in dispersing the LC in a chemically different isotropic

Figure 1. Drawings by Lehmann of droplet textures that wind and rotate under the action of an increasing temperature gradient (from left to right) (adapted from Ref. [10]).

liquid in which it is not fully miscible (certainly the method used by Lehmann). In that case, the LC must however be partly miscible to the isotropic liquid to observe a Lehmann effect [17,18]. In the following, we discuss separately the case of the cholesteric droplets coexisting with their own isotropic liquid, the case of the cholesteric emulsions and the case of the nematic droplets coexisting with their own isotropic liquid.

3.1. Cholesteric droplets coexisting with their own isotropic liquid

In this section, we are dealing with the cholesteric droplets observed in the coexistence region between the cholesteric phase and its isotropic liquid. Both diluted cholesteric LCs (nematic phase doped with a small amount of a chiral dopant, less than 5% by weight in general) and compensated cholesteric LCs (nematic phase usually doped with a large concentration – 50 wt% typically – of cholesteryl chloride (CC) [19]) are considered. In both cases, the cholesteric pitch is of the order of a few micrometers to a few tens of micrometers. In practice, the cholesteric LC is introduced between two parallel glass plates and the temperature gradient is imposed perpendicularly to the surface of the glass plates. Depending on the authors, the plates can be chemically treated or not. A classical treatment consists in depositing by spin coating a thin polymercaptan layer. This treatment, which we systematically used in our group in Lyon, was shown to give a sliding planar anchoring in the cholesteric phase [20]. In addition, we observed that the cholesteric phase tends to dewet on the polymercaptan layer in the coexistence region, which favors the formation of the droplets. Bare glass plates can also be used but the results are less reproducible from our point of view because of a tendency of the droplets to stick on the glass. Most experiments in the group of Y. Tabe in Tokyo were performed in this way [21–23]. Other surface treatments were also used occasionally. We will mention a treatment with DMOAP [24] which favors homeotropic anchoring [25] and a treatment with an azobenzene polymer (PEO-PAzo) which reduces the friction between the droplets and the surface after UV illumination [26]. These treatments can be used to change the orientation of the droplets with respect to the temperature gradient [24].

3.1.1. Main textures

Four main types of droplets have been studied: the banded and concentric-circle (CC) droplets, the double-twist (DT) droplets and the twisted bipolar (TB) droplets. Their typical radius ranges from a few micrometers to a few tens of micrometers. The banded, CC and DT
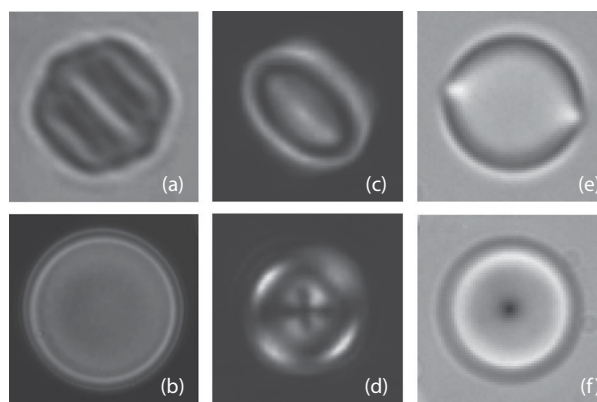

Figure 2. Typical texture of the cholesteric droplets observed experimentally in the coexistence region with the isotropic liquid. (a) Banded droplet (natural light); (b) Concentric-circle (CC) droplet (crossed polarizers); (c) Double-twist (DT) droplet with its revolution axis parallel to the glass plates (crossed polarizers); (d) Double twist (DT) droplet with its revolution axis perpendicular to the glass plates (crossed polarizers); (e) Twisted-bipolar (TB) droplet with its revolution axis parallel to the glass plates (natural light); (f) Twisted-bipolar (TB) droplet with its revolution axis perpendicular to the glass plates (natural light). Photos (c) and (d) have been taken from Ref. [22] and reprinted by permission of the Physical Society of Japan. The typical radius of these droplets ranges from a few μm to a few tens of μm depending on the cholesteric pitch.

droplets are observed when the preferred orientation of the director at the cholesteric-isotropic interface is tilted by about 45–70° with respect to the normal to the interface, while the bipolar droplets are observed when the orientation is planar. Classical LCs such as MBBA or the cyanobiphenyls of the homologous series of the nCB and nOCB give a tilted anchoring [27] while LC such as CCN37 gives a planar anchoring [28,29]. Figure 2(a) shows a typical banded droplet. In this micrograph, the helix is perpendicular to both the bands and the direction of observation. Optical analysis showed that the helix is little deformed in the bulk of the droplet [30]. By contrast, the helix is distorted close to the surface because of the tilted anchoring. This leads to the formation of a virtual disclination line on the surface [29]. Figure 2(b) shows a CC droplet. This droplet is just a banded droplet observed along its helical axis. This can be directly checked by submitting a CC droplet to a vertical electric field parallel to the helical axis. If the LC is of positive dielectric anisotropy, this orientation of the helix is less energetically favorable than the horizontal orientation corresponding to a banded droplet. For this reason the CC droplets should tilt and transform into banded droplets after the application of an electric field. This is shown in the movie S0. Note that in this example, the applied electric field is 10 times smaller than the critical field that should be applied to unwind the helix. For this
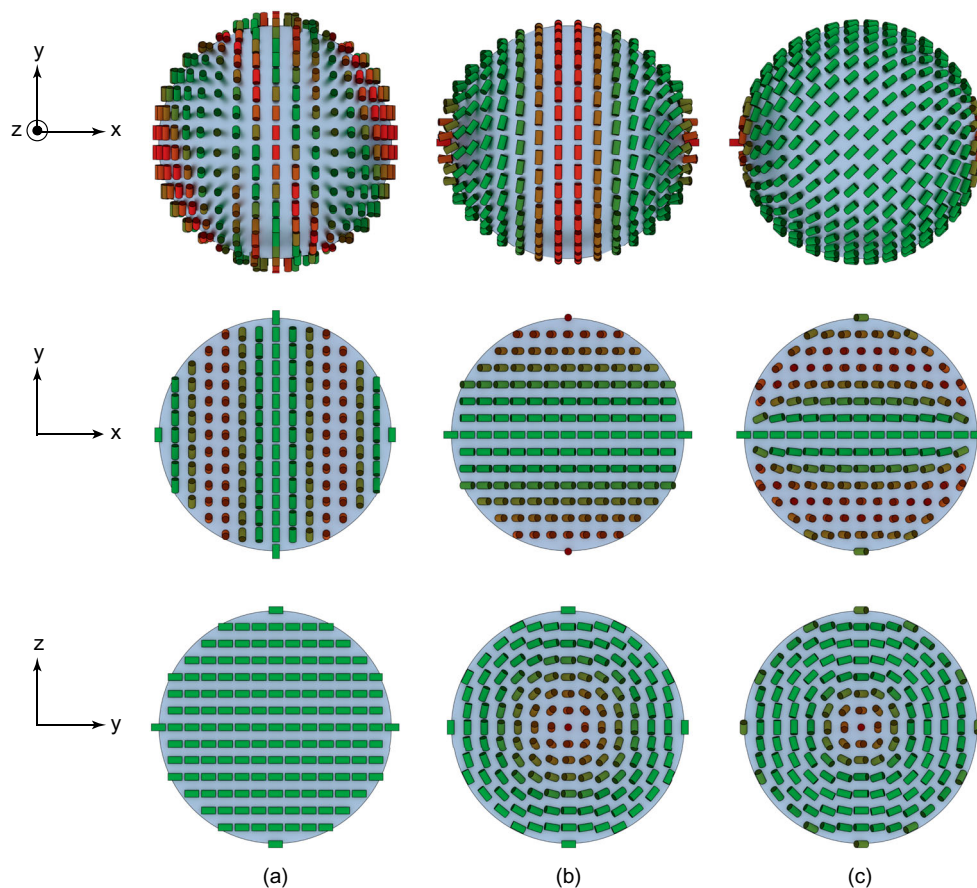
Figure 3. (a) Director field inside a banded (or CC) droplet; (b) Director field inside a DT droplet; (c) Director field inside a TB droplet. The first line shows top views of the director field for different types of droplets. The cylinders are red (green) at places where the anchoring is broken (satisfied). The second and third lines show the director field in the horizontal and vertical planes, respectively. The cylinders are painted in green (red) when the director is parallel (perpendicular) to the plane of the figure.

reason, the cholesteric pitch does not significantly change during this operation.

For completeness, we mention that similar droplets with an intermediate orientation of the helical axis were also observed when the glass plates are treated with DMOAP [24]. Figure 2(c) (Figure 2d) shows a DT droplet when its revolution axis is parallel (perpendicular) to the direction of observation. In such a droplet, a virtual disclination line forms along the equator, i.e. the great circle perpendicular to the revolution axis of the director field, because of the tilted anchoring on the surface [29]. In practice, the banded droplets transform into DT droplets when their radius is comparable to or smaller than the cholesteric pitch [23,29]. Finally, Figure 2(d) (Figure 2e) shows a TB droplet [28] when the axis joining the two surface point defects is perpendicular (parallel) to the direction of observation. In this droplet, the director field is radially twisted perpendicularly to this axis. A schematic representation of the director field inside the three types of droplets is shown in Figure 3.

3.1.2. Role of the temperature gradient

In most experiments, the temperature gradient is imposed by placing the sample between two ovens regulated at different temperatures. An experimental setup of this type is described in Ref. [16]. Another possibility is to dope the LC with a dye and to illuminate the sample with a laser beam with a wavelength in the absorption band of the dye. In that case, significant local temperature gradient can appear and produce thermomechanical effects [26,31,32].

When a temperature gradient $\vec{G}$ is imposed to the sample, all the droplets which are not rotationally invariant around an axis parallel to $\vec{G}$ start rotating in the same direction, provided that they are not attached to a surface or blocked by a dust particle (one such droplet is visible in video S1). This applies to the banded and CC droplets (Figure 2(a,b), respectively) and to the DT and TB droplets when their revolution axis is perpendicular to the temperature gradient (Figure 2c,e, respectively). This is the Lehmann effect. Apart from the CC droplets, the rotation is directly observable in natural light under
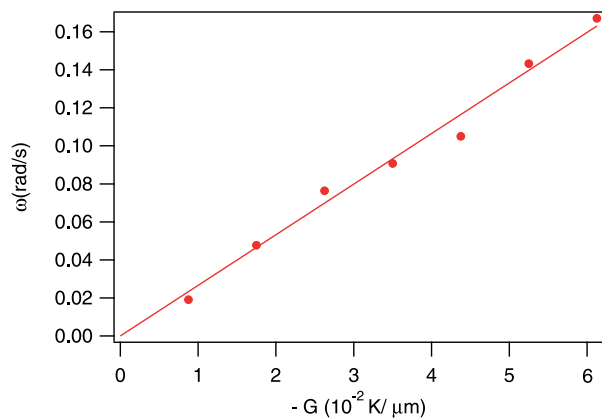
Figure 4. Angular rotation velocity as a function of the temperature gradient for banded droplets of diameter 10 μm (four bands typically). Mixture of 8OCB +50 wt% CC. Sample thickness: 25 μm. Cholesteric pitch: 6 *μ*m. Data from Ref. [16]. Reprinted with permission from Phys. Rev. Lett., 100, 217802 (2008). Copyright 2008, American Physical Society.

the microscope, because the texture rotates. This is not the case with the CC droplets which must be observed between crossed polarizers to detect the rotation of the helix. In that case, the transmitted intensity oscillates with a period equal to a quarter of the period of rotation of the helix. This rotation of the helix was also observed by fluorescence confocal polarizing microscopy (FCPM) [24]. The sense of rotation reverses if the temperature gradient is reversed. Video S1 shows the rotation of banded droplets in a diluted mixture 7CB + 0.6% R811. In this experiment, the cholesteric pitch is positive (right-handed cholesteric), close to 14 μm. When the sample, of thickness 56 μm, is heated from below and observed from the top, all the droplets rotate anticlockwise. This means that the rotation vector of the droplets and the temperature gradient are of opposite signs, a general property in all right-handed cholesteric LCs. Of course, the rotation vector of the droplets and the temperature gradient are of the same sign in all left-handed cholesteric LCs. The angular rotation velocity ω is also proportional to the imposed temperature gradient (Figure 4). This property is general and was observed with all the types of droplets [16,22,28,33,34].

3.1.3. Shape of CC and banded droplets
The shape of the droplets can be determined by two methods. The first one is an optical method consisting in measuring the intensity transmitted between crossed polarizers across a CC droplet. The theoretical value of the transmitted intensity can be calculated and compared to the experiment. This experiment was performed with the mixture CCN37 + 0.57 wt% R811 under moderate temperature gradients. The glass plates were treated with

a polymercaptan layer. A comparison between the experimental transmission curves and the theoretical curves led to the conclusion that the droplets were spherical as long as their diameter was smaller than the sample thickness [29,34]. The second method consists in using a fluorescence confocal polarizing microscope to reconstruct the director field inside the droplets [24]. In this experiment, the cholesteric mixture composed of 73.7 wt% MLC-2039 + 24.5 wt% 8CB + 1.8 wt% R811 was used and the glass plates were covered with a polymercaptan layer. The main conclusion of this study was that banded and CC droplets were spherical within the uncertainties and were attached to the colder glass plate with a large contact angle (Figure 5). This shows that the cholesteric LC slightly wets the colder glass plate, even when it is coated with a polymercaptan layer.

3.1.4. Role of the droplet size
We only consider here droplets which are not confined, i.e. whose diameter is less than the sample thickness. In that case, several behaviors are observed depending on the type and orientation of the droplets. For the DT (Figure 2c), CC (Figure 2b) and TB (2e) droplets, the period of rotation increases linearly with the radius. This is shown in Figure 6(a)–(c), respectively [22,28,35]. We will note that the smallest increase is observed with the CC droplets, for which the velocity is almost constant. By contrast, the period of rotation of the banded droplets increases much faster, as it increases almost quadratically with the radius. This is shown in Figure 6(a) [22,35].

3.1.5. Role of the concentration of chiral molecules and of the equilibrium twist
For more clarity, we will discuss separately the case of the diluted cholesteric LCs and the case of the compensated cholesteric LCs that contain a single type of chiral molecule.

• Diluted cholesteric LCs
They are obtained by doping a nematic LC with a chiral molecule whose concentration C is lower (or even much lower) than 8–10 wt%. In these mixtures, the Helical Twist Power, defined to be HTP $= 1/PC$, is constant, meaning that the equilibrium twist $q = 2\pi/P$ where P is the cholesteric pitch, is proportional to C. The HTP also changes sign when one changes enantiomer and strongly depends on the chemical nature of the chiral molecule. Hence the questions: Does the rotation velocity reverse when one changes enantiomer, does it depend on the concentration of chiral molecules and does it depend on the chemical nature of the chiral molecules or only on their HTP?
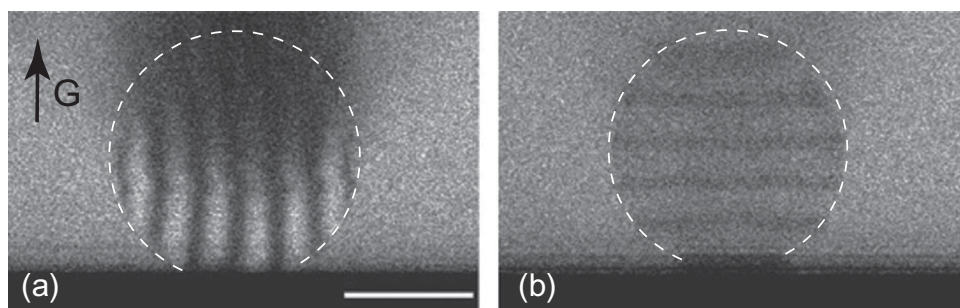
Figure 5. FCPM images of a banded droplet (a) and a CC droplet (b) in a vertical temperature gradient. The bands perpendicular to the helical axis are clearly visible. The two droplets are almost spherical and slightly truncated on the side in contact with the cold plate. The white bar is 10 μm long (photos taken from Ref. [24]).
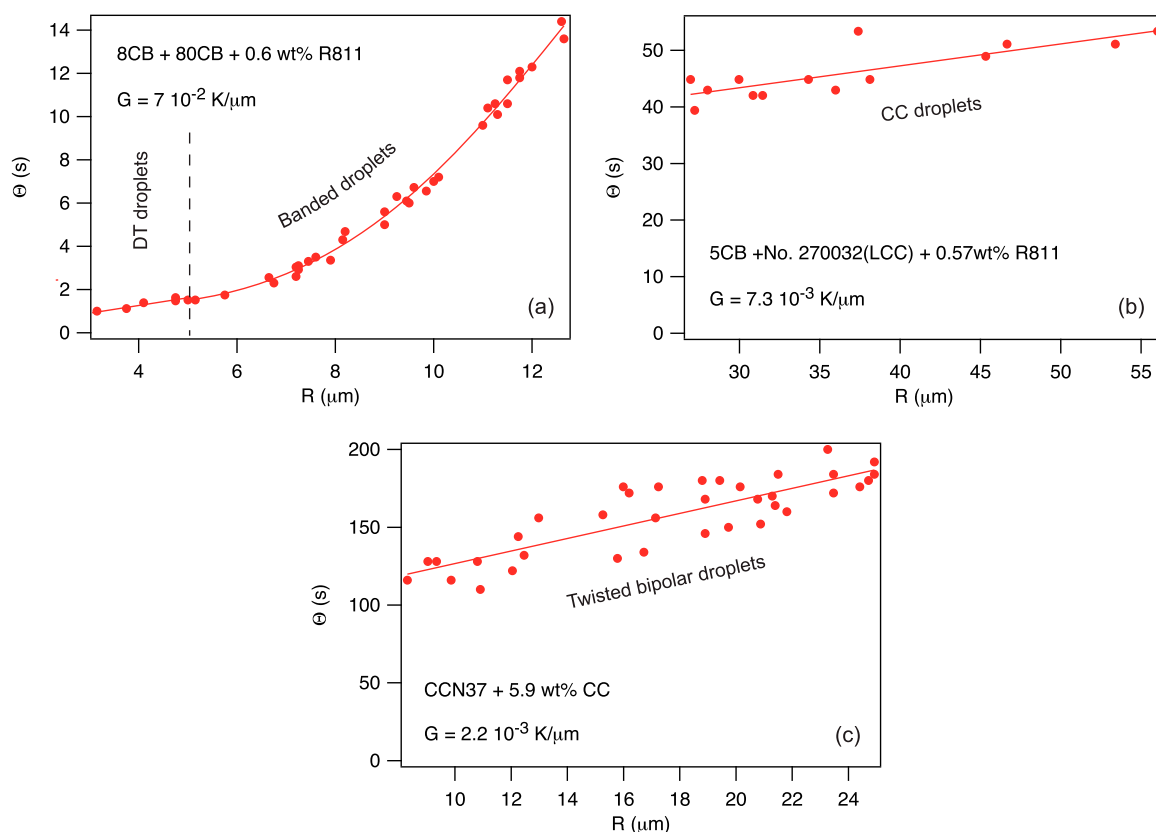

Figure 6. Period of rotation $\Theta = 2\pi/\omega$ as a function of the droplet radius. (a) DT and banded droplets. The vertical dashed line indicates the transition between these two types of droplets. The solid line is the best fit with a linear law for the DT droplets and with a law of the type $a + bR^2 + cR^4$ for the banded droplets. The data have been taken from Ref. [35] with kind permission of The European Physical Journal; (b) CC droplets. The solid line is the best fit with a linear law. The data have been taken from Ref. [21] and reproduced by permission of The Royal Society of Chemistry; (c) Twisted bipolar droplets. The solid line is the best fit with a linear law. The data have been taken from Ref. [28].

The answer to the first question is 'yes' as we have checked by changing enantiomers (in our case by replacing R811 by S811).

The answer to the second question was given by measuring the ratio ω/G for droplets of the same radius as a function of concentration. The result is that the rotation velocity of the DT and CC droplets [22] (Figure 7a) and of the twisted bipolar droplets [28] (Figure 7b) linearly increases with concentration, whereas the velocity of the banded droplets has a more complex behavior, decreasing first quadratically [22,35] (this is shown in Figure 7a) before increasing again above 5 wt% typically (with the R811) [35].

The answer to the third question was given by measuring the rotation velocity of droplets in compensated mixtures obtained by mixing the LC with two chiral dopants
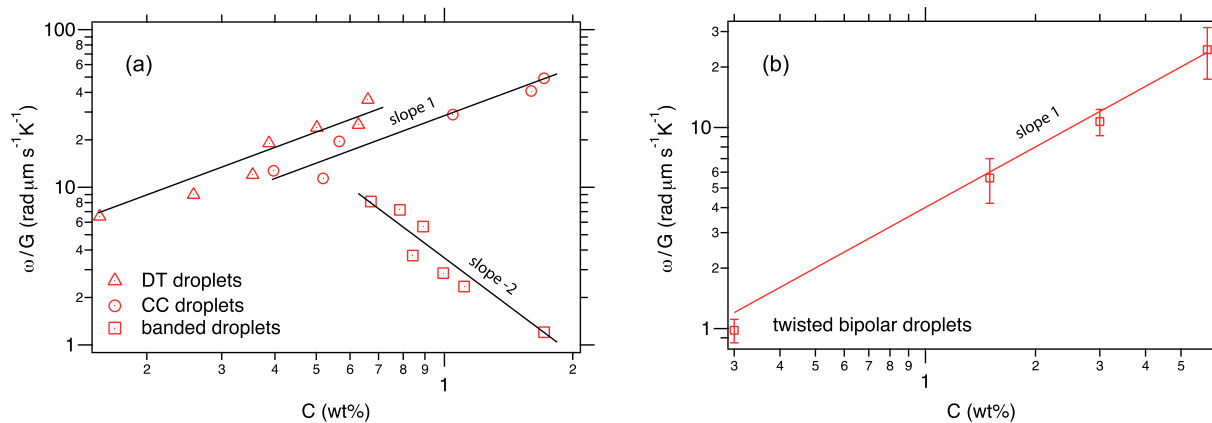
Figure 7. Ratio ω/G as a function of the concentration of chiral molecules for different types of droplets of similar radius. In (a) the radius of the droplets was $\sim 15\,\mu m$ for the CC and banded droplets and $7.5\,\mu m$ for the DT droplets. The LC was a mixture of 5CB and LC No. 270032 from LCC, Japan, in the weight ratio 3:2. The chiral molecule was the R 4-[[(1-methylheptyl)oxy]carbonyl]phenyl 4-(hexyloxy)benzoate. Data taken from Ref. [22] reprinted by permission of the Physical Society of Japan. In (b), the radius of the bipolar droplets was $\sim 15\,\mu m$. The LC was CCN37 and the chiral molecule was the CC.

of opposite handedness which are not enantiomers of each other. The main result of these experiments was that the rotation velocity vanishes when the mixture is compensated (i.e. when the pitch is infinite) and the director field is not twisted [36]. Note that the symmetry group of the phase at the compensation point in these mixtures is not $D_{\infty h}$ as in usual nematics, but D_{∞} because the phase remains chiral (no mirror symmetry and no inversion center) if the two chiral dopants are not enantiomers of each other. This important observation shows that only the macroscopic twist of the director field is important, independently on the chemical nature of the chiral molecules. In particular, it is not sufficient to have a chiral phase to observe a Lehmann effect.

• Compensated cholesteric LCs

It is still possible to prepare a compensated cholesteric LC by just mixing a nematic LC with a single chiral dopant. In practice, very few chiral dopants have this property, the best known being the cholesteryl chloride (CC) used in most experiments. In that case, the equilibrium twist varies rapidly with temperature and changes sign at the compensation temperature at which it vanishes. Note that at this temperature the symmetry group of the cholesteric phase changes from D_2 to D_{∞} as in the previous compensated mixtures. By changing the concentration of CC, it is possible to prepare a cholesteric mixture in which the compensation temperature is either larger (in which case it is virtual) or smaller than the clearing temperature. With the eutectic mixture 8CB/8OCB (EM), the critical concentration $C^{\star}$ of CC at which these two temperatures coincide is close to 42 wt%. If $C > C^{\star}$, the pitch is positive while it is negative when $C < C^{\star}$. By measuring in the mixture EM+CC the rotation velocity of banded droplets
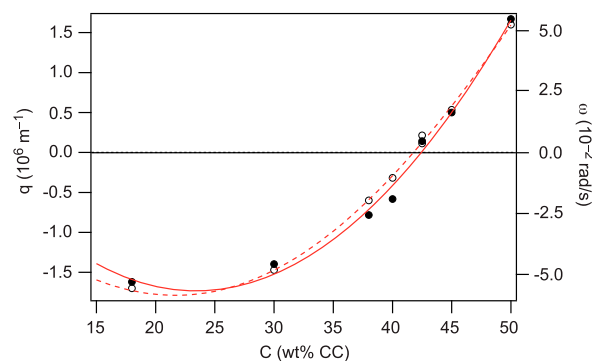

Figure 8. Equilibrium twist (empty circles) and angular rotation velocity (solid circles) at $G = -0.0175\,K/\mu m$ of droplets of radius R such as $qR = 5$ as a function of the concentration of CC (EM 8CB/8OCB+CC). This graph has been recalculated from the data given in Ref. [30] and reproduced with kind permission of *The European Physical Journal*. Within the experimental errors, q and ω vanish at the same concentration of CC.

as a function of the concentration of CC, it was found that the droplets stop rotating within the experimental errors when $C = C^{\star}$ [30].[1] On the other hand, the droplets rotate anti-clockwise when $C > C^{\star}$ ($P > 0$) and clockwise when $C < C^{\star}$ ($P < 0$) when the sample is heated from below (see Figure 8). This means that – as in all the diluted cholesteric mixtures studied so far – the rotation vector and the temperature gradient are oriented in the same direction when $q < 0$ (left-handed cholesteric) and in opposite directions when $q > 0$ (right-handed cholesteric). In addition, it was observed that the rotation velocities measured in the mixture EM+CC were comparable to the rotation velocities found in diluted mixtures of similar equilibrium twist, despite a much smaller concentration of chiral molecules in the latter (up to 1000
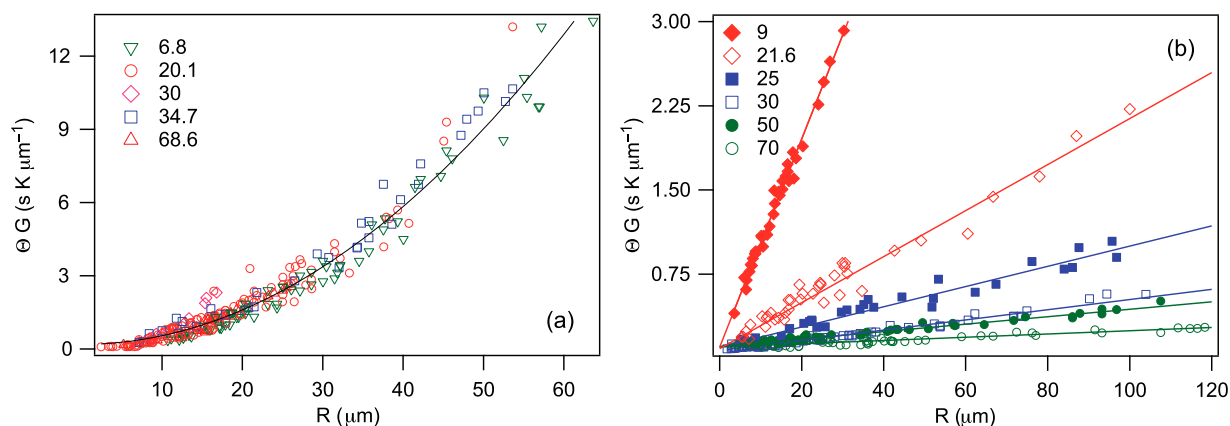
Figure 9. Product ΘG as a function of the radius for banded (a) and CC (b) droplets. Each symbol corresponds to a different thickness given in μm in each graph. Mixture MBBA + 1 wt% R811. These data have been obtained with temperature gradients ranging from 0.009 to 0.027 K/μm. Data taken from Ref. [38]. Reprinted with permission from Phys. Rev. E, 91, 032502 (2015). Copyright 2015, American Physical Society.

times less). These results provide a new confirmation that only the macroscopic twist of the phase is important in the Lehmann effect.

3.1.6. Thickness effect

Several studies have shown that the droplets are almost spherical when their apparent diameter is smaller than the sample thickness. However, the droplets must take the shape of a pancake when their diameter is larger than the sample thickness and this should influence their rotation velocity.

To study these confinement effects, diluted cholesteric mixtures of MBBA + R811 were used [37,38]. In these mixtures, banded droplets form spontaneously and they can be reoriented into CC droplets by applying an AC electric field parallel to the temperature gradient. Indeed, MBBA is of negative dielectric anisotropy [39] so that the helix orients parallel to the field. Systematic studies have shown that the rotation velocity of the banded droplets – whether or not confined – is almost independent of the sample thickness (Figure 9a) whereas the rotation velocity of the CC droplets strongly decreases when the sample thickness decreases, even when they are not confined (Figure 9b). It must be emphasized that this effect is independent of the electric field intensity and of its frequency chosen in the dielectric regime, which means that the field reorients just the molecules and the helix. A thickness effect was also observed with the TB droplets. For these droplets, the velocity is independent of the thickness when they are not confined, but strongly decreases when they are confined and the thickness decreases [28,34].

The texture of the droplets can also change drastically under confinement. One example is shown in Figure 10 where we can see two droplets strongly confined in which
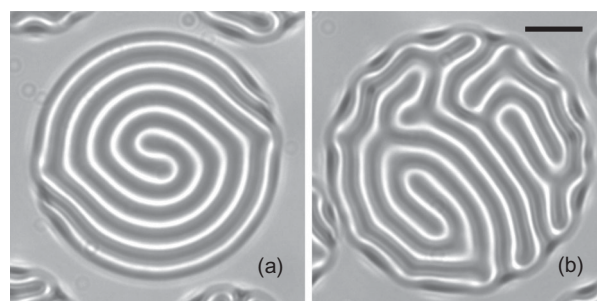

Figure 10. Two droplets strongly confined in a sample of thickness $d = 6.8\,\mu$m. The bar is 20 μm long. Mixture MBBA + 1 wt% R811 of pitch $P \approx 10.4\,\mu$m. Reprinted with permission from Phys. Rev. E, 91, 032502 (2015). Copyright 2015, American Physical Society.

the bands form a double spiral and a labyrinth. These droplets are different from classical banded droplets shown in Figure 2(a) and rotate at different velocities, the former rotating twice faster than the latter which surprisingly rotates at the same velocity as the usual banded droplets. This example again shows the importance of the texture on the rotation velocity. Another spectacular example was given recently by Bono et al. [40–42] who observed the aggregation of isolated DT droplets in samples of thickness $d < P$ (Figure 11(a–c)). Because these aggregates have radii much larger than the pitch, they are strongly confined as illustrated in Figure 11(d). These aggregates also rotate clockwise when the sample is heated from below, which means that $\vec{\omega}$ and $\vec{G}$ are here of the same sign. This sense of rotation is the same as in classical droplets because the cholesteric phase is here left-handed (S811 was used in this experiment). Finally, it was observed that the rotation velocity of the aggregates strongly decreases when their aggregation number N – and thus their radius – increase. This dependence
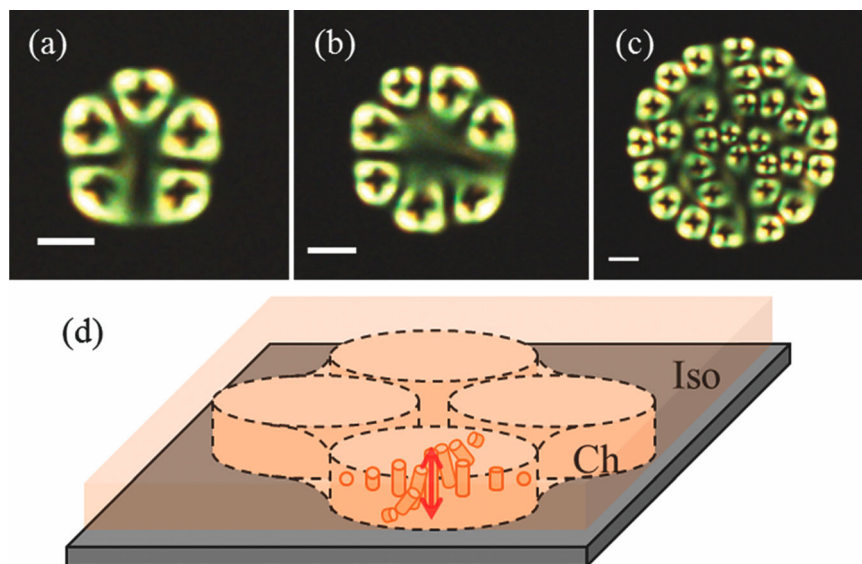
Figure 11. Aggregates of DT droplets in a sample of thickness ~15 μm. Mixture RDP-V0639 + 0.71 wt% S811 + 2.1 wt% PEO-PAzo of pitch $P \approx -12.8$ μm. The scale bars are 10 μm long (from Ref. [40], reproduced by permission of The Royal Society of Chemistry).

resembles very much the one observed with the banded droplets.

3.1.7. Hydrodynamic effects

An important question, which is still under debate, is to determine what is rotating in the droplets. Is it just the texture, as claimed by Lehmann himself, which would imply that only the orientation of the molecules changes or the whole droplets which would mean that they rotate as rigid bodies.

To answer this question, a photobleaching experiment was conducted first in the group of Tabe [21] and then in our group in Lyon [43]. In this experiment, the cholesteric LC is doped with a fluorescent molecule. The dye is then bleached locally by focusing a laser either directly inside a droplet [21,43] or in its close vicinity in the isotropic liquid [43]. Observation by fluorescence microscopy of the time evolution of the bleached spot allows one to follow the motion of its center of gravity and to know if the fluorescent dye is advected – or not – by a flow during the rotation of the droplet. In this way, Yoshioka et al. [21] arrived to the conclusion that banded droplets were rotating as rigid bodies, whereas only the texture is rotating in CC droplets. These results are important because they suggest the existence of two different mechanisms for the rotation of the CC and banded droplets.

However, we never detected under the microscope a rotational flow around the banded droplets and yet we observed thousands of droplets. For this reason, we redid the photobleaching experiment. Doing this, we found that for CC [43] and TB droplets [28], only the texture
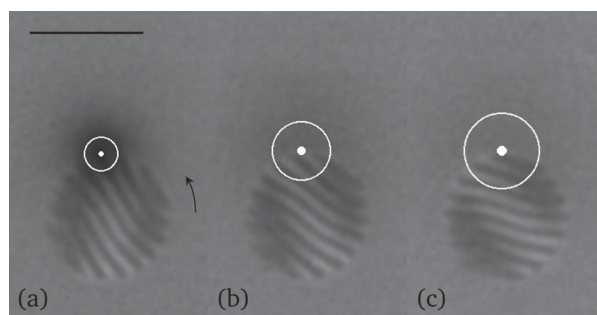
Figure 12. Time evolution of the bleached spot during the rotation of a banded droplet. During the 20 s separating photo (a) and photo (c) the droplet rotates by ~40 degree. By contrast, the center of mass of the spot (reconstructed with a tailored signal processing algorithm and marked by a white dot) does not move when the dye diffuses. This shows that only the texture is rotating (from Ref. [43], reproduced by permission of The Royal Society of Chemistry).

rotates. This result was obtained by directly observing the time evolution of bleached spots inside and outside of the droplets. For the banded droplets, the experiment was done in a somewhat different manner [43], by observing the evolution of spots situated between the droplets and the isotropic liquid. In that case, only the part of the spots situated in the isotropic liquid was analyzed to not be disturbed by the optical distortions due to the banded structure. In this way, we found that there was no flow in the isotropic liquid and we concluded from this observation that the droplets could not rotate as rigid bodies. Videos S2, S3 and S4 taken from our own experiments, as well as Figure 12 for the case of a banded droplet, show these results quite clearly. Note that this technique does

not allow one to explore the flows in the sample thickness. So we cannot exclude for the moment the existence of convective rolls in the sample thickness in the coexistence region.

These observations were recently completed by Nishiyama et al. [44] who observed banded droplets in a cholesteric sample in which micron-size particles were dispersed. Doing this, they observed that the particles in the isotropic liquid do not move, even when they are very close to the surface of the droplets. By contrast, a particle attached to the surface of a droplet rotates with the same velocity as the droplet. The authors conclude from this observation that the banded droplets rotate as rigid bodies and that a thin layer of isotropic liquid with a very low viscosity exists at their surface to explain the absence of observable flow in the isotropic liquid in their near vicinity.

This interpretation is rather surprising from our point of view. For this reason, we propose to interpret differently this observation as simply due to the existence of an anchoring force between the particle and the droplet that drives the particle during the rotation of its internal texture. Indeed, the director orientation must change at the surface of the droplet. For this reason, the anchoring energy of the particle on the surface of the droplet depends on its position on the droplet and is minimal at some places which are well defined with respect to the bands.[2] As a consequence, the particle experiences a force when it shifts from these positions, which happens when the internal texture of the droplet rotates. In that case, the particle will also rotate if this force can equilibrate the viscous friction force acting on it.

To check whether this interpretation makes sense, let us estimate the order of magnitude of these forces. In experiments, the particle of radius $R \sim 1\,\mu$m moves with velocity $v \sim 1\,\mu$m/s and experiences a viscous friction force $6\pi\eta R v$ of the order of $0.4\,$pN by taking $\eta \sim 0.02\,$Pa.s. In practice the anchoring force varies from 0 to some maximum value of the order of $W_a R$ where W_a is the anchoring energy of the director at the surface of the particle. The particle will thus rotate with the droplet if $W_a R > 0.4\,$pN which imposes $W_a > 4 \times 10^{-7}\,$J/m^2. This value corresponds to an anchoring extrapolation length K/W_a (where $K \sim 2\,$pN is the Frank constant just below the cholesteric/isotropic transition for cyanobiphenyls-based LC mixture [45]) of the order of 5 µm, which is considered as a very weak anchoring in the literature. In practice, the anchoring is certainly stronger (for rough or treated surfaces, the anchoring length can be as low as $\sim 10\,$nm [46,47]), meaning that the pinning must be very efficient. This fortifies our interpretation. For this reason, we would be a little less emphatic than Nishiyama et al. [44] and Kitahata [48]

before claiming that the banded droplets rotate as rigid bodies. In our opinion, the banded droplets behave as the CC and TB droplets and do not rotate as rigid bodies. Only their internal textures rotate as Lehmann already pointed out in 1921 [13].

3.1.8. Impurity effects

In practice, it is often useful to increase the freezing range of the cholesteric mixture to stabilize the droplets. Indeed, the smaller the freezing range is, the more unstable the droplets are because of the temperature variations due to fluctuations in the temperature controllers. This is the case for instance in the mixture 7CB + 1 wt% R811 where the freezing range is of the order of 0.02°C with pure 7CB. In that case, the measurements are difficult because the droplets constantly change size even by controlling to within 0.01°C the temperature of the ovens used to impose the gradient. One way to solve this problem is to use a commercial eutectic mixture instead of 7CB, in which case the freezing range is much larger – of the order of 1°C or more. Another possibility is to dope the pure LC with a known impurity to increase the freezing range in a controlled way. In that case, one can ask whether the Lehmann effect changes? To answer this question, a mixture of 7CB + 1 wt% R811 was doped with different impurities at different concentrations. Nonmesogenic impurities such as the biphenyl (BP), the hexachloroethane (HCE) and the fluorinated polyether polymer PF-656 [49] were used as well as a mesogenic impurity, the LC I52 [50]. Typical phase diagrams are shown in Figure 13. As we can see, the partition coefficient of the nonmesogenic impurities is less than 1 whereas the one of the I52 is larger than 1. With these mixtures, the rotation velocity of the banded droplets was systematically measured at different concentrations [51]. The main result was that the rotation velocity of the droplets depends on the nature of the impurity and on its concentration. However, this dependence can be easily rescaled by plotting the product $qG\Theta/\gamma_1$ as a function of qR as shown in Figure 14. That means that the variations of the rotation velocity are mainly due to variations of the equilibrium twist q and of the viscosity γ_1.

3.2. Emulsified cholesteric droplets

Up to recently, no one was able to observe the Lehmann rotation in an emulsified cholesteric phase. Indeed, the droplets do not rotate under a temperature gradient when they are suspended in usual liquids such as water, glycerol or mineral and silicon oils. It must be emphasized that the LCs are generally rather insoluble in these liquids. This situation changed recently when Yoshioka and Araoka used as dispersing liquid the PF-656 [49], a fluorinated
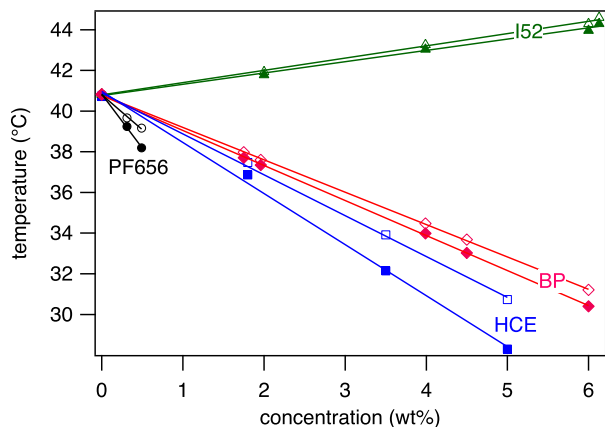
Figure 13. Phase diagrams of the mixture 7CB + 1 wt% R811 doped with different impurities (from Ref. [34,51] except for the phase diagram with the PF656 which has been measured again). Open (closed) symbols correspond to the liquidus (solidus) line.
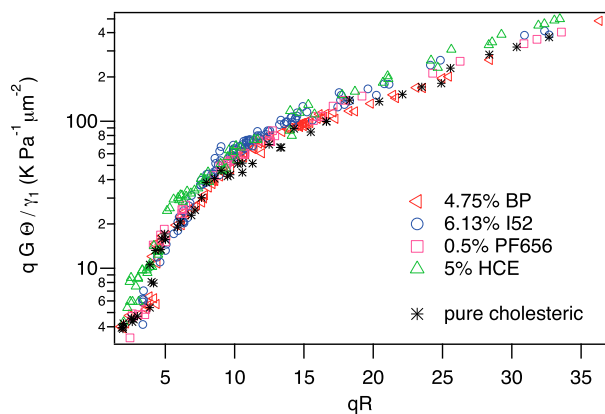

Figure 14. Product $qG\Theta/\gamma_1$ for banded droplets as a function of the dimensionless radius qR. All points fall on the same master curve whatever the nature of the impurity used to dope the cholesteric mixture 7CB + 1 wt% R811. This graph has been calculated from the data given in Refs. [34,51].

Figure 15. Angular velocity (in absolute value) as a function of the droplet radius for the main types of droplets observed in the samples: spiraling droplets (a), quadrupolar droplets (b) and banded droplets (c). All photos have been taken in natural light. The bar is 10 μm long. Filled and open symbols have been measured with temperature gradient of opposite signs (from Ref. [18], reproduced by permission of The Royal Society of Chemistry).

polyether oil in which their LC – the eutectic mixture E8 doped with 0.8 to 2 wt% S811 – was partly miscible [17]. With this system, these authors prepared emulsions of cholesteric droplets and observed that their texture could rotate very fast, typically 10 times faster than in conventional experiments realized in the coexistence region between the LC and its own isotropic liquid. In addition, the Lehmann effect can be observed in the entire range of existence of the cholesteric phase. To understand the origin of this spectacular effect, we reproduced a similar experiment by using the cholesteric mixture 7CB + 1.27 wt% R811. With this mixture, we found very similar results to those of Yoshioka and Araoka. In particular, we observed that – as in conventional experiments in the coexistence region – the rotation velocity of the droplets is proportional to the temperature gradient and is strongly dependent on the texture and radius
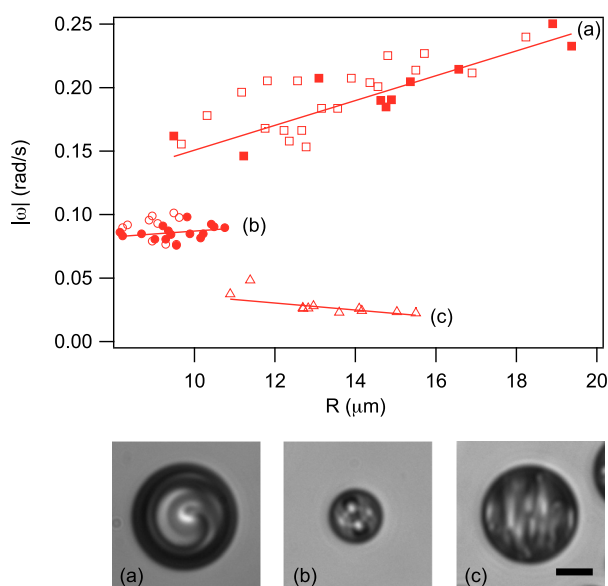
of the droplets. This is shown in Figure 15 for three different types of droplets: spiraling droplets, quadrupolar droplets and banded droplets. Note that the name of these droplets was given in reference to their aspect in natural light – shown in the insets in Figure 15. These droplets are different from the ones shown in Figure 2 because of the homeotropic anchoring of the director at the interface with the PF-656. Their structure, discussed in Refs. [17,52–55], is still controversial and we will not discuss this delicate point in this review. We will also note that for all the droplets, $\vec{\omega}$ and $\vec{G}$ are of opposite signs (of the same sign) when a right-handed (left-handed) cholesteric LC is used. This is the same as in the classical Lehmann effect. More interestingly, it was observed that convective rolls were present across the sample thickness when a temperature gradient was applied to the sample. These flows were directly visualized by adding colloidal particles in the PF-656 and by following their motion under the microscope. Video S5 shows their convective motion in the vicinity of a rotating spiraling droplet. As we can see, the particles mainly move across the sample thickness and do not rotate in the plane of the sample. This shows that the droplets do not rotate as solid bodies in this experiment. These convection rolls are generated by a Marangoni stress at the surface of the droplet, itself due to a large temperature variation of the surface tension between the LC
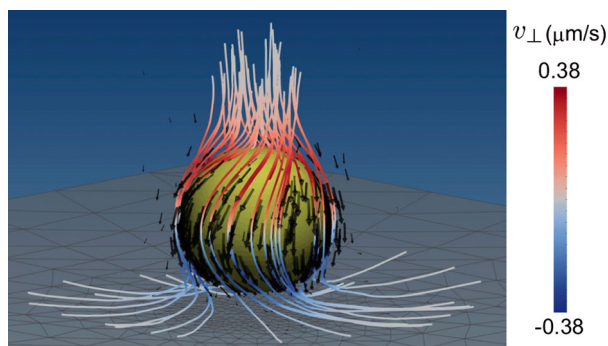
Figure 16. Field lines of the Marangoni flow around a cholesteric droplet dissolving in a surfactant solution. Here, $v_\perp$ is the orthoradial component of the velocity. (Reprinted with permission from Phys. Rev. E, 99, 022704 (2019). Copyright 2019, American Physical Society.)

and the PF-656 [18]. This strong dependence is clearly due to the fact that the LC is partly miscible in this oil. The Marangoni flows were also indirectly evidenced by observing the migration of the droplets parallel to the glass plates when a temperature gradient was applied parallel to the glass plates [18,56]. We also found that these flows and the Lehmann rotation simultaneously disappear when glycerol is used instead of PF-656. In this case we checked that the surface tension was almost constant [18]. These observations clearly show that the Lehmann rotation of the cholesteric droplets in PF-656 is due to the Marangoni flows.

Finally, we mention that the rotation of the cholesteric droplets was also observed by Yamamoto and Sano [57] during their dissolution in a surfactant solution. In this experiment, no temperature gradient was applied. However, a strong Marangoni flow was still detected by following by PIV with a confocal microscope the motion of fluorescent microspheres dispersed in the surfactant solution. In this case, the surface tension variation responsible for the Marangoni stress is due to a gradient in surfactant concentration at the surface of the droplet. With this technique, these authors were able to reconstruct the projection of the velocity field in the horizontal plane at different heights in the sample thickness. Their main result was that the velocity has a small orthoradial component that changes sign on both sides of the equatorial plane of the droplet (see Figure 16). The authors also showed numerically that this flow can be described as the superposition of a Stokeslet, a source dipole and a Rotlet dipole on the vertical axis of the droplet (see Ref. [58] for the definition of a Stokeslet/Rotlet). These observations confirm that the particles rotate in the sample thickness by remaining in the same vertical plane on average over time. This excludes the presence of a solid rotation of the droplets around a vertical axis although their texture

rotates very fast. These experiments confirm that the rotation of the emulsified cholesteric droplets is due to a coupling with Marangoni flows.

3.3. Nematic droplets coexisting with their own isotropic liquid

By symmetry, a droplet cannot rotate in a temperature gradient if it is superposable to its image in a mirror parallel to the temperature gradient. This means that a nematic droplet can rotate if and only if its director field breaks this mirror symmetry. This is the case with the twisted bipolar droplets that can spontaneously form in some nematic LCs (most notably lyotropic chromonic nematic LCs [59], but also in some very specific thermotropic nematic LCs [60–62]) with a giant elastic anisotropy when the anchoring is planar at the surface of the droplets. This was found theoretically by Williams [61] when the twist constant K_2 is much smaller than the splay and bend constants K_1 and K_3. In these droplets, the director field is similar to the one described in Figure 2(e,f) except that it can be twisted to the right or to the left with the same probability because the phase is not chiral. The previous experiments with cholesteric LC have shown that only the macroscopic twist of the director field is important. For this reason, one can expect that twisted nematic droplets also rotate in a temperature gradient, in one sense or in the other depending on the sign of the twist. To test this prediction, twisted bipolar nematic droplets were prepared with a chromonic LC that is known to have a giant elastic anisotropy [63]. In practice aqueous solution of SSY with a molar concentration ranging between 0.88 and 1 mol/kg was used. We recall that SSY (of molar mass 452 g) is a food dye known under the name Sunset Yellow (E-110 in Europe). With this mixture, it was observed that the droplets were rotating in both directions under a temperature gradient when the axis joining the two surface point defects is perpendicular to the temperature gradient [64]. This is shown in Figure 17 and in video S6. It was also observed that their period of rotation Θ was inversely proportional to the temperature gradient and proportional to their radius (Figure 18). This experiment is important because it confirms that the molecules and the phase do not need to be chiral to observe the Lehmann effect. Only the macroscopic twist of the director field is important. This twist can develop spontaneously at equilibrium as in cholesteric phases or be induced by a confinement effect as in the case of the droplets described in this paragraph.

3.4. The inverse Lehmann effect

We end this experimental section by mentioning an intriguing work of Sato and coworkers about the inverse
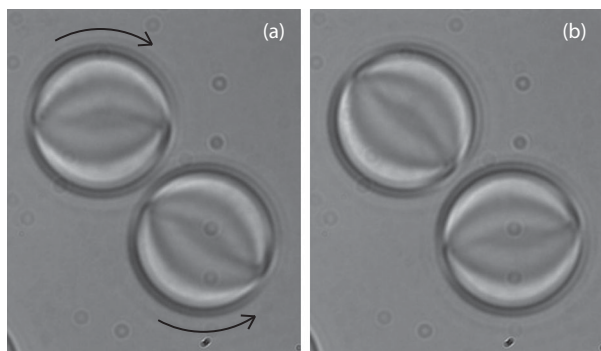
Figure 17. Two twisted bipolar droplets of radius 25 μm rotating in opposite directions when they are subjected to a temperature gradient perpendicular to the glass plates ($G = 0.84$ mK/μm): (a) $t = 0$; (b) $t = 10$ s. (Reprinted with permission from Phys. Rev. Lett., 117, 057801 (2016). Copyright 2016, American Physical Society.)

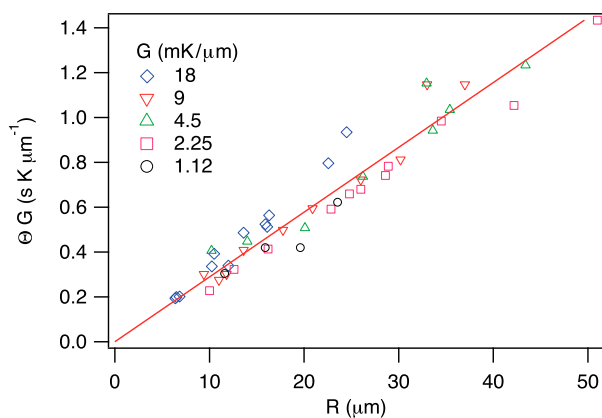**Figure 18.** Product ΘG as a function of the droplet radius R (adapted from Ref. [64]). (Reprinted with permission from Phys. Rev. Lett., 117, 057801 (2016). Copyright 2016, American Physical Society.)

Lehmann effect [65]. In this experiment, the authors impose a rotating electric field to cholesteric droplets in the coexistence region. Doing this, the droplets are forced to rotate at the same angular velocity as the electric field. In parallel, the authors detect a flux of heat across their sample, which changes sign when the sense of rotation of the droplets is reversed. This observation suggests the existence of an inverse Lehmann effect. On the other hand, the measured effect is much stronger than the one expected from the classical irreversible thermodynamics theory [66].

3.5. Summary of the main experimental results

To summarize, the Lehmann effect of cholesteric and nematic LCs has been observed both in the zone of coexistence with the isotropic liquid close to the clearing temperature of the LC, and in emulsions at all temperatures on condition that the LC is partly miscible in the dispersing liquid. In all cases, the rotation velocity of the droplets is proportional to the temperature gradient and it changes sign when the temperature gradient is reversed. The droplets are usually spherical when they are not confined, which is the case when their apparent diameter is smaller than the sample thickness. The rotation velocity only depends on the macroscopic twist q of the director field. The twist can be induced either by introducing a chiral molecule (usual case of the cholesteric LCs) or by a confinement effect in the very anisotropic nematic phases (case of the chromonic LC). In the cholesteric LCs, the rotation velocity changes sign when one changes the enantiomer. In the nematic phase, the two senses of rotation are simultaneously observed. In all cases, the rotation vector and the temperature gradient are of the same sign when $q < 0$ and of opposite signs when $q > 0$. The rotation velocity strongly depends on the texture and on the radius of the droplets. For the CC, DT and TB droplets observed in the coexistence region, the rotation velocity decreases as $1/R$ while for the banded droplets and the aggregates of DT droplets it decreases as $1/R^2$. In emulsions, linear dependences are rather observed, with a large (moderate) velocity increase in the case of the spiraling (quadrupolar) droplets and a large velocity decrease in the case of the banded droplets. The rotation velocity also depends on the twist q of the director field (proportional to the concentration C of chiral molecules in diluted cholesteric LCs). More precisely, the rotation velocity of the CC, DT and TB droplets increases linearly with q, whereas the velocity of the banded droplets decreases as $1/q^2$ (provided C is not too large). There are also thickness effects dependent on the type of the droplets. For instance, the rotation velocity of the banded droplets in the coexistence region depends very little on the thickness, even when they are strongly confined. By contrast, the rotation velocity of the CC droplets increases when the thickness increases, even when they are not confined. More important, the rotation velocity of the droplets in the coexistence region does not depend on the nature and the concentration of the impurities used to increase the freezing range of the mixture. Finally, strong Marangoni flows have been detected in the case of emulsions. These flows are clearly responsible for the rotation of the droplets, because the droplets stop rotating when they are absent. The situation is more confuse in the coexistence region, except for CC droplets for which everybody agrees that only the texture rotates. The case of the banded droplets is still under debate, with some researchers describing solid body rotation while others finding texture rotation only.

4. Theoretical models

These experiments suggest that several mechanisms may be responsible for the Lehmann rotation. In the case of emulsions, the rotation is clearly due to Marangoni flows because the rotation stops when they disappear. The situation is much more confusing when the droplets coexist with their own isotropic phase, because in that case, such flows seem to be absent. If so, another origin must be found. One of them was proposed as early as 1968 by Leslie in the framework of nematodynamics in terms of thermomechanical coupling [15]. This model, which became a paradigm, can be generalized to nematics by taking into account texture-dependent thermomechanical terms (first derived by Akopyan and Zel'dovich [67] and later reformulated by Pleiner and Brand [68]). It can also be declined in several versions discussed in the next three sections. We will show that, against all expectations, this classical model cannot explain the Lehmann effect for multiple reasons, and therefore that a different theoretical framework is needed when studying rotating chiral droplets.[3] The next model discussed in the fourth section is completely different. It is based on a melting-growth (MG) process that could explain both the spherical shape and the rotation of the droplets in the coexistence region. This model has nevertheless not yet been fully explored because of its complexity. Finally, we will present in the fifth section a purely hydrodynamic model based on the existence of Marangoni flows. This model clearly applies to emulsions, i.e. to cholesteric droplets dispersed in a liquid that partly dissolves the LC. We will show that it can broadly explain the observations in these systems. By contrast, it is not clear whether it can be applied to droplets in coexistence with their isotropic phase.

4.1. The thermomechanical models

In a nematic or a cholesteric LC several unusual out-of-equilibrium cross-coupling effects exist, which vanish in ordinary liquids. These effects are associated with the existence of a hydrodynamic variable that does not exist in ordinary fluids, the director **n** which is the unit vector giving the mean orientation of the molecules at each point. In practice the director defines the optical axis of the medium and can experience a torque. This torque may be induced by an external field such as an electric or magnetic field or by a flow. If the phase is chiral or if the director field is distorted, the director can also experience a torque when the LC is subjected to a temperature gradient. This torque, first predicted by Leslie [15] in cholesterics and later by Akopyan, Zel'dovich, Pleiner and Brand in distorted nematics [67,68] has been proposed

as the driving force for the Lehmann effect. This torque was also observed in molecular dynamics simulations by Sarman and coworkers [69–71]. Two models based on the existence of this torque have been proposed in the literature, which we discuss in the next two paragraphs. In the first model, which we used in Refs. [16,33,64,72], only the texture rotates and there is no flow, while in the second model used by Tabe and coworkers [21,40–42] and Yamamoto and coworkers [24] it is assumed that the droplet rotates as a rigid body.

4.1.1. First model of texture rotation without flow driven by Leslie, Akopyan and Zel'dovich thermomechanical torques (TM1 model)

The main assumptions of this model are that only the texture rotates without flow of the molecules. This assumption is clearly not verified in cholesteric in PF-656 emulsions but seems reasonable in the coexistence region, at least in the case of the CC droplets for which everyone agrees that there is no visible flow [21,43]. Under this assumption it is possible to derive an exact formula for the rotation velocity of the droplets.

To obtain this formula, we first remark that if the droplet and its internal texture remains unchanged during the rotation, its total free energy, which includes the bulk elastic energy and the surface anchoring energy, must remain constant. As a result,

$$\frac{\mathrm{d}}{\mathrm{d}t}\left(\iiint_{\text{drop}} f\,\mathrm{d}^3\vec{r} + \iint_{\text{drop}} W\,\mathrm{d}^2\vec{r}\right) = 0, \qquad (1)$$

where $f(n_i, n_{i,j})$ denotes the elastic Frank energy density [39] and $W(n_i)$ the anchoring energy at the surface of the droplet. If the anchoring energy and the elastic constants are independent of temperature – and so of time –, f and W only depend on $\vec{n}(x, y, z, t)$. After derivation with respect to $\vec{n}$ under the integral and one integration by parts, one obtains

$$\iiint_{\text{drop}} -\vec{h} \cdot \frac{\partial \vec{n}}{\partial t}\,\mathrm{d}^3\vec{r} + \iint_{\text{drop}} \left(\frac{\delta W}{\delta \vec{n}} - \underline{\underline{C}}\vec{v}\right)$$
$$\cdot \frac{\partial \vec{n}}{\partial t}\,\mathrm{d}^2\vec{r} = 0, \qquad (2)$$

where $\vec{h} = -\delta f/\delta \vec{n}$ is the molecular field of components $h_i = (\mathrm{d}/\mathrm{d}x_j)(\partial f/\partial n_{i,j}) - (\partial f/\partial n_i)$, $\underline{C}$ the elastic surface torque tensor of components $C_{ij} = \partial f/\partial n_{i,j}$ and $\vec{v}$ the unit vector normal to the surface of the droplet and directed outwards. Taking into account the torque balance equation at the surface of the droplet,

$$\frac{\delta W}{\delta \vec{n}} - \underline{\underline{C}}\vec{v} = 0, \qquad (3)$$

and the fact that $\partial \vec{n}/\partial t$ is perpendicular to $\vec{n}$ since $\vec{n}$ is a unit vector, we get

$$\iiint_{\text{drop}} \vec{h}_\perp \cdot \frac{\partial \vec{n}}{\partial t} \, d^3\vec{r} = 0, \qquad (4)$$

where $\vec{h}_\perp$ is the component of $\vec{h}$ orthogonal to $\vec{n}$. We emphasize that this equation is very general and also applies in the presence of flows on condition that the elastic constants and the anchoring energy are independent of temperature.

We then write the bulk torque equation for the director. If there is no flow, this equation reads [39,73]:

$$\gamma_1 \frac{\partial \vec{n}}{\partial t} = (\underline{I} - \vec{n} \otimes \vec{n})(\vec{h} + \vec{f}_{TM}) \qquad (5)$$

Here, $\underline{I}$ is the identity matrix, $\otimes$ denotes the dyadic product of two vectors (with $(\vec{a} \otimes \vec{b})_{ij} = a_i b_j$), γ_1 is the rotational viscosity and $\vec{f}_{TM}$ is the thermomechanical force on the director which can be written in the form

$$\begin{aligned} \vec{f}_{TM} = {}& \bar{\xi}_1 (\vec{\nabla} \cdot \vec{n})\vec{G} + (\bar{\xi}_2(\vec{n} \cdot \vec{\nabla} \times \vec{n}) + \nu)(\vec{n} \times \vec{G}) \\ & + \bar{\xi}_3(\vec{n} \cdot \vec{G})((\vec{\nabla} \times \vec{n}) \times \vec{n}) \\ & - \bar{\xi}_4 \vec{\nabla} \cdot (\vec{G} \otimes \vec{n} - \vec{G} \cdot \vec{n}\underline{I}). \end{aligned} \qquad (6)$$

Note that $\vec{f}_{TM}$ includes the classical Leslie term (proportional to ν) [39,73,74], as well as four 'texture dependent' terms (proportional to $\bar{\xi}_i, i = 1 - 4$) first introduced by Akopyan and Zel'dovich [67] and recalculated more rigorously by Pleiner and Brand[4] [68]. The correspondence with the formulation of Akopyan and Zeldovich and that of Pleiner and Brand is given in Refs. [72,75].

We then multiply the torque equation (5) by $\partial \vec{n}/\partial t$ and we integrate over the whole droplet. This gives, by using Equation (4) after noting that $\vec{h}_\perp = (\underline{I} - \vec{n} \otimes \vec{n})\,\vec{h}$:

$$\gamma_1 \iiint_{\text{drop}} \left(\frac{\partial \vec{n}}{\partial t}\right)^2 dV = \iiint_{\text{drop}} \vec{f}_{TM} \cdot \frac{\partial \vec{n}}{\partial t} \, d^3\vec{r}. \qquad (7)$$

Finally, we note that if the texture remains unchanged during the rotation, one must have [16,33]

$$\frac{\partial \vec{n}}{\partial t} = \omega \vec{e}_z \times \vec{n} - \omega \frac{\partial \vec{n}}{\partial \theta}, \qquad (8)$$

where $\vec{e}_z$ is the unit vector along the z-axis, chosen normal to the glass plates and parallel to the temperature gradient with $\vec{G} = G\vec{e}_z$, and θ the polar angle in cylindrical coordinates (r, θ, z). By replacing $\partial \vec{n}/\partial t$ by its expression (8) in Equation (7) and by setting $\delta\vec{n}/\delta\theta = \partial\vec{n}/\partial\theta - \vec{e}_z \times \vec{n}$, we finally obtain by assuming that the temperature gradient is uniform, along the z-axis ($\vec{G} = G\vec{e}_z$):

$$\omega = -G\frac{\nu L_\nu + \bar{\xi}_1 q L_1 + \bar{\xi}_2 q L_2 + \bar{\xi}_3 q L_3}{\gamma_1 L_\gamma} \qquad (9)$$

with the dimensionless integrals

$$\begin{aligned} L_\gamma &= \frac{1}{V}\iiint_{\text{drop}} \left(\frac{\delta\vec{n}}{\delta\theta}\right)^2 dV, \\ L_\nu &= \frac{1}{V}\iiint_{\text{drop}} (\vec{n} \times \vec{e}_z) \cdot \frac{\delta\vec{n}}{\delta\theta} \, dV, \\ L_1 &= \frac{1}{qV}\iiint_{\text{drop}} (\vec{\nabla} \cdot \vec{n})\,\vec{e}_z \cdot \frac{\delta\vec{n}}{\delta\theta} \, dV, \\ L_2 &= \frac{1}{qV}\iiint_{\text{drop}} (\vec{n} \cdot \vec{\nabla} \times \vec{n})\,(\vec{n} \times \vec{e}_z) \cdot \frac{\delta\vec{n}}{\delta\theta} \, dV, \\ L_3 &= \frac{1}{qV}\iiint_{\text{drop}} (\vec{n} \cdot \vec{e}_z)\big([\vec{\nabla} \times \vec{n}] \times \vec{n}\big) \cdot \frac{\delta\vec{n}}{\delta\theta} \, dV, \end{aligned} \qquad (10)$$

where V is the volume of the droplet.

Formula (9) shows that the rotation velocity is proportional to the temperature gradient in agreement with experiments. It also predicts that ω is proportional to the thermomechanical constants ν and $\bar{\xi}_i$ ($i = 1$–3) and is inversely proportional to γ_1.

Finally, these formulas can be used to estimate the rotation velocity of the different types of droplets as a function of their radius. This calculation gives for the CC and banded droplets by assuming that they are spherical and the cholesteric helix is not distorted inside:

$$\omega = -\frac{\bar{\nu}G}{\gamma_1} \quad \text{for CC droplets,} \qquad (11)$$

$$\omega = -\frac{\bar{\nu}G}{\gamma_1(1 + \frac{2}{5}q^2 R^2)} \quad \text{for banded droplets,} \qquad (12)$$

where we set $\bar{\nu} = \nu - \bar{\xi}_2 q$. Note that the calculation for the banded texture is valid for a particular position (or phase shift) of the helix in the droplet. For arbitrary values of the phase shift ψ, the calculation can be done as well and the impact of ψ becomes rapidly negligible when $qR \gg 1$.

For the nematic twisted bipolar droplet, ω can be calculated by using an ansatz for the director field combining a pure bipolar configuration $\vec{n}_b$ with a pure concentric configuration $\vec{n}_c$, namely $\vec{n}_{tb} = \vec{n}_b \cos(\alpha) - \vec{n}_c \sin(\alpha)$ with $\alpha(\rho) = \alpha_0 \rho/\rho_0$. Here, ρ is the radius of the cylindrical coordinates local to the droplets (ρ, φ, ζ), with the ζ axis taken along the bipole, and $\rho_0 = \sqrt{R^2 - \zeta^2}$ ($-R \le \zeta \le R$). The angle α_0 fixes the twist inside the droplet (inset in Figure 19). With this director
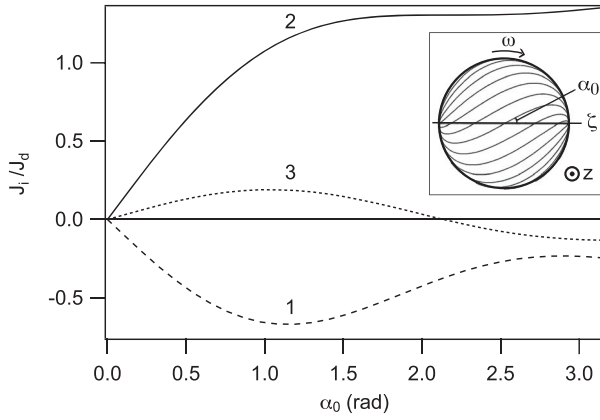
Figure 19. Ratios of the splay ($i = 1$), twist ($i = 2$) and bend ($i = 3$) integrals J_i over the dissipation integral J_d as a function of the twist angle α_0. The value of i is indicated besides each curve. Inset: angle α_0 and director surface field lines in a twisted bipolar droplet. The ζ axis is the bipole axis and the z axis is perpendicular to the glass plates and parallel to the temperature gradient. (Reprinted with permission from Phys. Rev. Lett., 117, 057801 (2016). Copyright 2016, American Physical Society.)

field, we calculate

$$\omega = -\frac{G}{\gamma_1 R} \frac{\sum_i \bar{\bar{\xi}}_i J_i(\alpha_0)}{J_d(\alpha_0)}, \tag{13}$$

where

$$J_1 = \iiint_{V_1} (\vec{\nabla} \cdot \vec{n}_{tb}) \left(\vec{e}_z \cdot \frac{\delta \vec{n}_{tb}}{\delta \theta} \right) d^3\vec{r}\,'$$

$$J_2 = \iiint_{V_1} (\vec{n}_{tb} \cdot \vec{\nabla} \times \vec{n}_{tb}) [\vec{n}_{tb} \times \vec{e}_z] \cdot \frac{\delta \vec{n}_{tb}}{\delta \theta} d^3\vec{r}\,'$$

$$J_3 = \iiint_{V_1} (\vec{n}_{tb} \cdot \vec{e}_z) [(\vec{\nabla} \times \vec{n}_{tb}) \times \vec{n}] \cdot \frac{\delta \vec{n}_{tb}}{\delta \theta} d^3\vec{r}\,'$$

$$J_d = \iiint_{V_1} \left(\frac{\delta \vec{n}_{tb}}{\delta \theta} \right)^2 d^3\vec{r}\,'. \tag{14}$$

Note that the integrals J_i (J_d), which are odd (even) functions of α_0, are made dimensionless by using the variables $x'_i \equiv x_i/R$ and are calculated over a spherical volume V_1 of radius unity. The calculated ratios J_i/J_d, evaluated using Mathematica, are shown in Figure 19 as a function of the surface twist angle α_0. They all vanish when $\alpha_0 = 0$, which means that $\omega = 0$ when the droplet is not twisted. The rotation velocity also changes sign when α_0, and so the twist of the director field, changes sign, in agreement with experiments (see Figure 17).

Finally, these formulas predict that the rotation velocity of the CC droplets is independent of R while that of the banded droplets approximately decreases as $1/R^2$ and that of the TB droplets decreases as $1/R$. These dependence are rather compatible with experimental observations although the rotation velocity of the

CC droplets is not strictly constant as we can see in Figure 6(b).

This model also predicts that the rotation velocity of the droplets should not depend on the sample thickness when they are not confined. This is reasonably the case for the banded droplets as shown in Figure 9(a). By contrast, the rotation velocity of the CC droplets tends to increase when the thickness increases (see Figure 9(b)) which is not predicted by the model.

Another weak point of the model comes from the order of magnitude of the rotation velocities calculated by taking the experimental values of the thermomechanical coefficients measured in the cholesteric phase [28,30,76–81]. For instance, in the compensated mixture 8CB/8OCB + 45 wt% CC the model predicts a rotation velocity which is typically 10 times smaller than the experimental one [30,82]. The disagreement can be much larger in diluted cholesteric phases where the predicted velocities are up to 1000 times smaller than the measured velocities [79,80]. The same was observed in the chromonic nematic LC where the rotation velocities calculated by taking typical values of $\bar{\bar{\xi}}$ found in the literature [28,67,83] are typically 100 to 10^4 times too small. The smallness of the predicted velocities is one of the main problems of this model.

Last but not least, the model does not always predict the good sense of rotation. This is observed in the compensated mixtures 8CB/8OCB + CC in which the sense of rotation of the banded droplets changes at a concentration of 43 wt% of CC (see Figure 8) corresponding to the compensation point of the cholesteric phase. By contrast, the coefficient $\bar{\nu}$ is always positive in these mixtures whatever the concentration of CC, so that the model always predicts the same sense of rotation in contradiction with experiments [30]. A similar problem was also observed in the diluted mixtures of 7CB doped with a few wt% of CC, in which the bad sense of rotation is also predicted by the theory [79,80].

For all these reasons, we think that the thermomechanical torques are not directly responsible for the Lehmann effect. As a consequence the Leslie paradigm – defined as the statement 'The Lehmann effect can be fully explained in terms of thermomechanical torque' – is wrong and another theoretical framework is needed for modeling the Lehmann rotation of LC droplets.

4.1.2. Second model of texture rotation coupled to a solid rotation of the droplets under the action of Leslie, Akopyan and Zel'dovich thermomechanical torques (TM2 model)

In the previous model, the velocity is obtained by balancing on average the internal thermomechanical torque with the internal viscous torque.

Another variant of the thermomechanical model has also been proposed in the literature by Tabe and coworkers [21,40–42] and used by other authors [24]. In this model, the authors suppose that the droplet rotates as a rigid body. We have already seen that this hypothesis is controversial from an experimental point of view. Nevertheless, let us assume that it is true. Because the velocity at the surface of the droplet no longer vanishes, the droplet must experience a torque $\vec{\Gamma}_\nu$ coming from the friction with the glass plates and the outer isotropic liquid. In the model of Tabe and coworkers, the rotation velocity of the droplet is then calculated by equilibrating this torque with the Leslie torque integrated over the whole droplet.

We claim that this calculation is incorrect and not consistent with the theory of nematodynamics, as we now demonstrate by applying the angular momentum theorem to the droplet [39]. According to this theorem,

$$\frac{\mathrm{d}\vec{M}_O}{\mathrm{d}t} = \iint_{\mathrm{drop}} \vec{r} \times \underline{\underline{\sigma}}\,\vec{v}\, \mathrm{d}S + \iint_{\mathrm{drop}} \underline{\underline{C}}\vec{v}\, \mathrm{d}S$$
$$+ \iiint_{\mathrm{drop}} \vec{\Gamma}^{\mathrm{ext}}\, \mathrm{d}V. \qquad (15)$$

In this equation, $\vec{M}_O$ is the angular momentum in O (origin of the laboratory frame of reference), $\underline{\underline{\sigma}}$ is the total stress tensor including the pressure term and the elastic, viscous and thermomechanical stresses, $\underline{\underline{C}}$ is the elastic surface torque tensor,[5] the expression of which is given in [39], $\vec{v}$ is the unit normal pointing out of the droplet and $\vec{\Gamma}^{\mathrm{ext}}$ is an external torque (in practice, a magnetic or an electric torque, but *not* the thermomechanical torque of Leslie, Akopyan and Zel'dovich associated with the thermomechanical stress[6]). Note that we excluded in Equation (15) contributions from external volume forces, since the only such force in this system is gravity, which cannot exert a torque on a spherical droplet of constant density.

Suppose now that the droplet is rotating as a solid at constant angular velocity. In that case, $\vec{M}_O$ is constant so that

$$\iiint_{\mathrm{drop}} \vec{\Gamma}^{\mathrm{ext}}\, \mathrm{d}V = - \iint_{\mathrm{drop}} \vec{r} \times \underline{\underline{\sigma}}\vec{v}\, \mathrm{d}S$$
$$- \iint_{\mathrm{drop}} \underline{\underline{C}}\vec{v}\, \mathrm{d}S. \qquad (16)$$

At the surface of the droplet, the boundary conditions impose that $\underline{\underline{\sigma}}\vec{v} = \underline{\underline{\sigma}}^{(I)}\vec{v}$ (balance of surface forces) and $\underline{\underline{C}}\vec{v} = \delta W/\delta\vec{n}$ (balance of surface torques) where $\underline{\underline{\sigma}}^{(I)}$ is the stress tensor in the isotropic liquid and W the anchoring energy. This allows us to rewrite the previous

equation as

$$\iiint_{\mathrm{drop}} \vec{\Gamma}^{\mathrm{ext}}\, \mathrm{d}V = - \iint_{\mathrm{drop}} \vec{r} \times \underline{\underline{\sigma}}^{(I)}\vec{v}\, \mathrm{d}S$$
$$- \iint_{\mathrm{drop}} \frac{\delta W}{\delta\vec{n}}\, \mathrm{d}S. \qquad (17)$$

In this equation, the second integral in the r.h.s. is the anchoring torque that the liquid exerts on the droplet. This torque must be equal to 0 by symmetry when the liquid is isotropic. As a consequence, the previous equation becomes simply[7]

$$\iiint_{\mathrm{drop}} \vec{\Gamma}^{\mathrm{ext}}\, \mathrm{d}V = - \iint_{\mathrm{drop}} \vec{r} \times \underline{\underline{\sigma}}^{(I)}\vec{v}\, \mathrm{d}S, \qquad (18)$$

where the integral in the r.h.s. is the viscous torque that the isotropic liquid exerts on the droplet. If the droplet is rotating as a solid, the continuity of the velocity at the surface of the droplet imposes that the isotropic liquid is sheared. As a consequence, this torque cannot vanish. This is possible if and only if the droplet experiences an external electric or magnetic torque. This was indeed observed experimentally with a nematic droplet subjected to a rotating electric field [84]. However, if this torque is equal to 0, the droplet cannot rotate as a solid, even if it is submitted to a temperature gradient. This ends our demonstration.

For these reasons, and because the Leslie torque cannot be considered as an external torque, we think that the model of Tabe and coworkers is incorrect from a theoretical point of view in the framework of the Ericksen–Leslie theory and must also be abandoned.

4.1.3. Third model of rotating texture 'surfing' on a heat wave in the absence of flow and thermomechanical coupling (TM3 model)

We have shown that the thermomechanical terms play a negligible role in the Lehmann effect and can be ignored. However, other terms involving the temperature dependence of the elastic constants and the anchoring energy could play a role. To prove this point theoretically, we now assume that f and W also depend on temperature. Doing this Equation (2) becomes

$$\iiint_{\mathrm{drop}} \left[-\vec{h} \cdot \frac{\partial\vec{n}}{\partial t} + \frac{\partial f}{\partial T}\frac{\partial T}{\partial t} \right] \mathrm{d}^3\vec{r}$$
$$+ \iint_{\mathrm{drop}} \left[\left(\frac{\delta W}{\delta\vec{n}} - \underline{\underline{C}}\vec{v} \right) \cdot \frac{\partial\vec{n}}{\partial t} + \frac{\partial W}{\partial T}\frac{\partial T}{\partial t} \right] \mathrm{d}^2\vec{r} = 0. \qquad (19)$$

If the texture rotates as a rigid body with an angular velocity ω one must have $\partial T/\partial t = -\omega(\partial T/\partial\theta)$. By using

Equation (3), we obtain instead of Equation (4):

$$\iiint_{\text{drop}} \vec{h}_\perp \cdot \frac{\partial \vec{n}}{\partial t}\, \mathrm{d}^3\vec{r} + \omega \left[\iiint_{\text{drop}} \frac{\partial f}{\partial T}\frac{\partial T}{\partial \theta}\, \mathrm{d}^3\vec{r} \right.$$
$$\left. + \iint_{\text{drop}} \frac{\partial W}{\partial T}\frac{\partial T}{\partial \theta}\, \mathrm{d}^2\vec{r} \right] = 0. \qquad (20)$$

If the thermomechanical terms and the flows are neglected, the bulk torque equation reads simply γ_1 $(\partial \vec{n}/\partial t) = \vec{h}_\perp$. By replacing $\vec{h}_\perp$ by its expression into the previous equation and by using Equation (8), we finally obtain the rotation velocity

$$\omega = -\frac{\iiint_{\text{drop}} \frac{\partial f}{\partial T}\frac{\partial T}{\partial \theta}\, \mathrm{d}^3\vec{r} + \iint_{\text{drop}} \frac{\partial W}{\partial T}\frac{\partial T}{\partial \theta}\, \mathrm{d}^2\vec{r}}{\gamma_1 L_\gamma}, \qquad (21)$$

where L_γ is given in Equation (10).[8] This calculation shows that it is not necessary to introduce the thermomechanical terms in the model to observe a rotation. However, it is only the orthoradial component of the temperature gradient (and not directly the vertical gradient) that is responsible for the rotation in this model. Because of this component, a rotating circular heat wave must exist on which the droplet surfs as a surfer on a wave at the sea. In practice, this component exists because of the anisotropy of the thermal conductivities and it must be proportional to the imposed temperature gradient. Another important point is that $\partial T/\partial \theta$ changes sign when q is changed to $-q$.[9] This model thus predicts that the sense of rotation is given by the sign of q, which is observed experimentally. Unfortunately, we do not know for the moment whether this model is pertinent in the coexistence zone because we do not know how the elastic constants and the anchoring energy change in this zone. Nevertheless we must emphasize that this model predicts a vanishing rotation velocity for the spherical CC droplets when the helix is not distorted inside. Indeed, in that case, it can be shown, by solving the heat equation, that the temperature gradient remains vertical inside the droplet, without orthoradial component. This is of course a shortcoming for this model, even if one could argue that this result is not rigorous because the helix is necessarily distorted near the surface because of the anchoring conditions. Further investigations are thus needed before concluding about the pertinency of this model.

4.2. The melting-growth model (MG model)

In this section, we only consider non-confined droplets with a diameter less than the sample thickness. So far, we assumed that the shape of the droplets was known. In emulsions, the droplets must be spherical because of the large surface tension between the LC and the dispersing liquid and their small size with respect the gravitational capillary length $\lambda_c = \sqrt{\gamma/\delta\rho g}$ where γ is the surface tension, g the gravity constant and $\delta\rho$ the density difference between the dispersing liquid and the LC. In the 7CB in PF-656 emulsions, for instance, $\lambda_c \approx 600\ \mu\text{m}$ by taking $\gamma = 10^{-3}$ N/m and $\delta\rho \approx 300$ kg/m^3 [18], which is indeed much larger than the diameter of the droplets in experiments.

By contrast, the spherical shape of the droplets observed in the coexistence region [24,29] is more surprising. This is not due to gravity, because in that case the gravitational length λ_c – of the order of 1 mm by taking $\gamma \approx 10^{-5}$ N/m [27,85] and $\delta\rho \approx 1$ kg/m^3 [86] – is still much larger than the diameter of the droplets observed in experiments. The problem comes from the fact that, in these experiments, we are dealing with diluted solutions of LC + impurity whose typical phase diagrams are shown in Figure 13. In these systems, the interface must satisfy the Gibbs–Thomson relation. This relation fixes the interface temperature as a function of its curvature and the local concentration of impurity and reads

$$T = T_c + mC_{Ii} - \frac{\gamma T_c}{\Delta H}\kappa, \qquad (22)$$

where T_c is the transition temperature of the pure LC, m the slope of the liquidus, C_{Ii} the impurity concentration at the interface (index 'i') in the isotropic liquid (index 'I'), ΔH the latent heat per unit volume and κ the curvature of the interface. Note that in this equation, we neglected the elastic corrections due the deformations of the director field [39,87]. This is justified in Ref. [51]. We recall that for a surface of revolution obtained by rotating a curve of equation $x = x(s), z = z(s)$ in the xz-plane about the z-axis (with s the arc length):

$$\kappa = \frac{1}{x}\frac{\mathrm{d}z}{\mathrm{d}s} - \frac{\mathrm{d}z}{\mathrm{d}s}\frac{\mathrm{d}^2x}{\mathrm{d}s^2} + \frac{\mathrm{d}x}{\mathrm{d}s}\frac{\mathrm{d}^2z}{\mathrm{d}s^2} \qquad (23)$$

with the constraint

$$\left(\frac{\mathrm{d}x}{\mathrm{d}s}\right)^2 + \left(\frac{\mathrm{d}z}{\mathrm{d}s}\right)^2 = 1. \qquad (24)$$

This equation gives the shape of the droplets provided that the wetting condition on the cold plate, the temperature field and the impurity concentration at the interface are known. In practice, the droplets dewet on the surface, in particular when it is treated with a polymercaptan layer (see Figure 5). The temperature field can be easily found if one assumes that the thermal conductivities of the two phases are equal. In that case, $T = T_b + Gz$ where T_b is the temperature of the bottom cold plate (we assume that the sample is heated from above). Finally, we can assume, by neglecting the Soret effect, that the
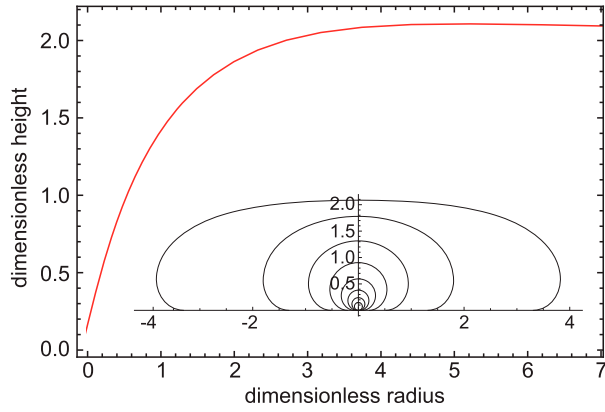
Figure 20. Height and shape of the droplets as a function of their radius calculated by solving numerically the Gibbs–Thomson equation at equilibrium. The lengths are given in unit of $L = \sqrt{L_c L_T}$. (Reprinted with permission from Phys. Rev. E, **98**, 032704 (2018). Copyright 2018, American Physical Society.)

impurity concentrations, denoted by C_I in the isotropic liquid and by C_{Ch} in the cholesteric (or nematic) phase, are constant and satisfy the relation $C_{Ch} = KC_I$ with K the partition coefficient of the impurity. This describes an equilibrium situation in which the bulk diffusion equations for the impurity are automatically satisfied as well as the equation of conservation of impurity at the interface as there is no flux of impurity in the two phases. Finally, the concentrations C_I and C_{Ch} are obtained by writing the global conservation of impurity in the sample. If V is the volume of the droplets and n their number per unit volume, this condition yields $nVC_{Ch} + (1 - nV)C_I = \bar{C}$ where $\bar{C}$ is the average concentration of impurity in the sample. Under these assumptions, it can be shown that the shape of the droplets depends on their relative size with respect to the typical length $L = \sqrt{L_c L_T}$ where $L_c = \gamma / \Delta H$ is the capillary length and $L_T = T_c / G$ the thermal length. More precisely, the droplets have an almost spherical shape if their radius $R < L$ and a flat shape when $R > L$ as shown in Figure 20. In the latter case, the height of the droplet saturates and cannot exceed $\sim 2L$ (Figure 20). This flattening is due to the temperature gradient.

It turns out that these predictions are not confirmed experimentally. Indeed, let us estimate the length L. By taking $\Delta H \approx 10^6$ J/m^3 [88] and $\gamma \approx 10^{-5}$ N/m [27,85] we calculate $L_c \approx 10^{-11}$ m $= 0.1$ Å. In typical experiments $G \approx 0.02$ K/μm and $T_c \approx 300$ K which gives $L_T \approx 0.015$ m. As a consequence $L \approx 4 \times 10^{-7}$ m $= 0.4\,\mu$m. This is very small, much smaller than the radius of the usual droplets observed experimentally. This shows that the surface tension in the coexistence region of diluted mixtures is not large enough to oppose the flattening effect of the temperature gradient at equilibrium.

This calculation is interesting because it shows that the almost spherical shape of the droplets observed in experiments is not an equilibrium shape. This calculation also shows that for these droplets, the capillary term in the Gibbs–Thomson equation is negligible with respect to the chemical term. As a consequence one must have at the surface of the droplets, by assuming that the thermal conductivities of the two are equal:

$$T = T_c + mC_{Ii} = T_b + Gz. \tag{25}$$

This relation shows that there must exist a gradient of impurity concentration at the surface of the droplet and thus inside, of the order of

$$(\nabla C)_{Ch} \sim K\frac{G}{m}. \tag{26}$$

The consequences of this chemical gradient are twofold.

It could first generate a chemomechanical torque on the director as underlined for the first time by de Gennes [73]. Such a torque exists and has already been observed in Langmuir monolayers [89–91], in smectic C* films [92] and even in cholesteric shells [93]. This torque could explain the Lehmann rotation of the droplets as long as it is large enough. In that case, a model similar to the thermomechanical model can be developed, in which the thermomechanical coefficients are replaced by chemomechanical coefficients [51]. This model, however, predicts that the rotation velocity must depend on the chemical nature of the impurity and must change sign when m changes sign. These two predictions are not confirmed experimentally, and for this reason, we think that this 'chemical' explanation is not relevant to model the Lehmann effect, except perhaps to explain a recent observation by Bono and coworkers about an inversion of the rotation velocity of the droplets when a sample doped with photosensitive molecules is illuminated with UV light [26]. But even in that case, it could be that this inversion is due to an artifact, namely a possible local inversion of the temperature gradient caused by a large local heating, as demonstrated in Ref. [51].

A second consequence of this gradient comes from the application of the law of conservation of impurity at the surface of the droplet, which reads

$$C_{Ii}(1 - K)\vec{v} \cdot \vec{v} = -D_I(\vec{\nabla} C)_I \cdot \vec{v} + D_{Ch}(\vec{\nabla} C)_{Ch} \cdot \vec{v}. \tag{27}$$

In this equation, $\vec{v}$ denotes the unit vector normal to the interface and directed from the nematic (or cholesteric) phase towards the isotropic liquid and $\vec{v}$ the growth velocity of the nematic (or cholesteric) phase. This equation shows that the quantity of solute which is rejected at the interface per unit time and surface is balanced by the diffusion currents in the two phases. If there is no flow in
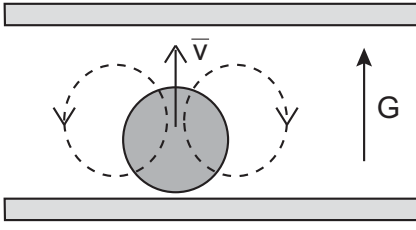
Figure 21. Hypothetical hydrodynamic flow induced by the presence of a droplet. In this model, the droplet keeps its stationary shape if the cholesteric phase melts at the top of the droplet and grows at the bottom. Because of this vertical motion, the internal texture of the droplet rotates (adapted from Ref. [51]).

the sample and the droplet has a stationary shape, we have necessarily $\vec{v} = 0$ which means that the two fluxes must equilibrate. This seems impossible to satisfy except if there is a vertical flow which drags at velocity $\bar{v}$ the droplet in the opposite direction as shown schematically in Figure 21. In order to estimate this velocity let us apply the previous equation at the top of the droplet. If this point is close to the top glass plate, one should have

$$D_I(\vec{\nabla} C)_I \cdot \vec{v} \approx 0, \qquad (28)$$

because there is no flux of impurity across the glass plate. By contrast, one has

$$D_{Ch}(\vec{\nabla} C)_{Ch} \cdot \vec{v} \sim K D_{Ch} \frac{G}{m}, \qquad (29)$$

according to Equation (26) which gives

$$\bar{v} = -v \sim -K D_{Ch} \frac{G}{m C_{Ii}(1-K)}, \qquad (30)$$

where C_{Ii} must be of the order of the average concentration $\bar{C}$ of impurity. This vertical motion of the droplet leads to an apparent rotation of its internal texture at angular velocity

$$\omega \sim -\bar{q}\,\bar{v} = \bar{q} K D_{Ch} \frac{G}{m\bar{C}(1-K)}, \qquad (31)$$

where $\bar{q}$ is the twist of the droplet in the vertical direction (proportional to q). This formula is interesting in many respects.

First, it predicts the good sense of rotation of the droplet whatever the impurity chosen. Indeed, the experiment shows that in all cases $\omega < 0$ when $q > 0$. This is the case for non-mesogen impurities for which $m < 0$ and $K < 1$ but also for the nematogen impurity I52 for which $m > 0$ and $K > 1$ (see the experimental section).

Second, it predicts that ω is proportional to G, which is observed in all experiments.

Third, it predicts that ω is proportional to the effective twist in the z-direction. This is compatible with experiments which show that the CC droplets in which the

helix is parallel to the temperature gradient rotate much faster than the banded droplets in which the twist is mainly in the direction perpendicular to the gradient. More precisely this formula predicts that the more tilted the helical axis with respect to the temperature gradient, the smaller must be the rotation velocity. This tendency was indeed observed experimentally by the authors of Ref. [24]. It must be emphasized here that the banded droplets never stop rotating in spite of the fact that the helical axis is perpendicular to the temperature gradient in the center of the droplets. The reason is that these droplets always exhibit double twist near their surfaces, as shown both theoretically and experimentally by confocal microscopy in Ref. [22]. This result was confirmed numerically in Ref. [29]. This particular structure induces a rotation of the edge of the droplets that extends to the whole texture because of the nematic elasticity. For this reason, the molecules must also rotate – and not only translate – inside these droplets. This molecular rotation induces a strong energy dissipation very similar to the one described in the thermomechanical model presented above [16,33]. This could qualitatively explain why the rotation velocity of the banded droplets is inversely proportional to γ_1 (see Figure 14 showing that all the points fall on the same master curve if and only if the period of rotation is divided by γ_1) and strongly decreases when their diameter increases. By contrast, the rotation velocity of the CC droplets must be independent of their diameter in this model, since no molecular rotation is necessary to observe the texture rotation. This is almost true when the droplets are not confined as we can see in Figure 6(b).

Fourth, it predicts the good order of magnitude for the rotation velocity of the droplets. To check this point, we can rewrite Equation (31) in the form

$$\Theta q G = \frac{2\pi \delta T}{D_{Ch}}, \qquad (32)$$

where $\delta T = m\bar{C}(K-1)/K$ is the freezing range. For CC droplet for which $\bar{q} = q$, experiments show that their velocity is the same as the one measured for the DT droplets at very small radius [38]. By using this remark and extrapolating the data of Figure 14, we deduce that for CC droplets $\Theta q G \approx 0.1\,\mathrm{K\,s\,\mu m^{-2}}$ by taking $\gamma_1 \approx 0.03\,\mathrm{Pa\,s}$ while the previous formula predicts $\Theta q G \approx 0.12\,\mathrm{K\,s\,\mu m^{-2}}$ by taking $\delta T = 1\,\mathrm{K}$ and $D_{Ch} = 50\,\mathrm{\mu m^2\,s^{-1}}$ [51].

On the other hand, the formula (32) suggests that the period of rotation increases when the freezing range increases, which is not observed, meaning that this oversimplified version of the model of melting-growth is incomplete and must be improved.

4.3. The model of texture rotation driven by Marangoni flows (H model)

In emulsions, the surface tension of the droplets is much larger than in the coexistence region with the isotropic phase of the LC and the spherical shape of the droplets just results from the minimization of their surface energy at fixed volume. In this case, experiments have shown that the droplets only rotate when convection rolls are present. It has been shown that these rolls are due to the existence of a Marangoni stress at the surface of the droplets induced by a surface tension gradient. In the experiments with the PF-656 [17,18], this gradient is generated by a temperature gradient, while in the experiments with surfactant solutions [57] it is due to a gradient of surfactant concentration. Although these flows have been detected experimentally only outside of the droplets, they must also develop inside the droplets in the form of a Hill vortex [94], by admitting that the cholesteric phase behaves to a first approximation as an isotropic liquid. We will see that these flows couple to the director and cause a texture rotation.

To show this result in the most general fashion, we start by establishing an exact relation between the angular velocity and the director and velocity fields.

To this purpose, we first note that if the droplet texture remains unchanged during the rotation, we have still

$$\frac{\partial \vec{n}}{\partial t} = \omega \vec{e}_z \times \vec{n} - \omega \frac{\partial \vec{n}}{\partial \theta}, \qquad (33)$$

and

$$\iiint_{\text{drop}} \vec{h}_\perp \cdot \frac{\partial \vec{n}}{\partial t} \, \mathrm{d}^3\vec{r} = 0, \qquad (34)$$

provided that the temperature variations of the elastic constants and the anchoring energy are negligible.

We then use the bulk torque equation by neglecting the thermomechanical torques:

$$\gamma_1 \frac{\partial \vec{n}}{\partial t} = \vec{h}_\perp - \gamma_2 \underline{\underline{A}} \vec{n} - \gamma_1 (\vec{v} \cdot \vec{\nabla}) \vec{n} + \gamma_1 \vec{\Omega} \times \vec{n}. \quad (35)$$

In this equation, $\vec{v}$ is the velocity, $\vec{\Omega} = \frac{1}{2} \vec{\nabla} \times \vec{v}$ is the local rotation rate, $\underline{\underline{A}}$ is the symmetric strain rate tensor of components $A_{ij} = \frac{1}{2}(v_{i,j} + v_{j,i})$ and $\gamma_1 \equiv \alpha_3 - \alpha_2$ and $\gamma_2 \equiv \alpha_3 + \alpha_2$ are two viscosities of the cholesteric phase (with α_2 and α_3 two of the five Leslie viscosity coefficients [39,73]).

Multiplying Equation (35) by $\partial \vec{n}/\partial t$ and integrating over the whole droplet gives, by using Equations (33)

and (34)

$$\omega = \frac{\iiint_{\text{drop}} (\gamma_2 \underline{\underline{A}} \vec{n} + \gamma_1 [(\vec{v} \cdot \vec{\nabla}) \vec{n} - \vec{\Omega} \times \vec{n}]) \cdot \frac{\delta \vec{n}}{\delta \theta} \, \mathrm{d}^3\vec{r}}{\iiint_{\text{drop}} \gamma_1 (\frac{\delta \vec{n}}{\delta \theta})^2 \mathrm{d}^3\vec{r}}, \tag{36}$$

where $\delta \vec{n}/\delta \theta \equiv \partial \vec{n}/\partial \theta - \vec{e}_z \times \vec{n}$ as before.

This expression can be simplified if the velocity field (and, consequently $\underline{\underline{A}}$) does not depend on θ. In this case (for a demonstration, see Ref. [18]),

$$\iiint_{\text{drop}} \underline{\underline{A}} \vec{n} \cdot \frac{\delta \vec{n}}{\delta \theta} \, \mathrm{d}^3\vec{r} = 0 \tag{37}$$

and ω takes the simplified form:

$$\omega = \frac{\iiint_{\text{drop}} [(\vec{v} \cdot \vec{\nabla}) \vec{n} - \vec{\Omega} \times \vec{n}] \cdot \frac{\delta \vec{n}}{\delta \theta} \mathrm{d}^3\vec{r}}{\iiint_{\text{drop}} (\frac{\delta \vec{n}}{\delta \theta})^2 \, \mathrm{d}^3\vec{r}}, \tag{38}$$

where γ_1 and γ_2 do no longer appear explicitly.

This expression can be used to estimate the rotation velocity of the droplets in emulsions. For instance, one calculates for a spherical droplet in which the helix is not distorted and makes an angle α with the z-axis [18]

$$\omega \approx \frac{5qR \sin^2 \alpha}{10 + (2q^2R^2 - 5) \sin^2 \alpha} \frac{G\gamma'}{2\mu + 3\mu'}. \tag{39}$$

This expression, valid for $qR \geq 4$ when the liquid and the LC have the same thermal conductivities, was obtained by approximating the velocity field by the one of a Hill vortex, of expression in polar coordinates (r, θ, z) [94]:

$$\begin{aligned} v_r &= -\beta rz \\ v_\theta &= 0 \\ v_z &= \beta(z^2 + 2r^2 - R^2). \end{aligned} \tag{40}$$

This vortex is schematically shown in Figure 22. In these expressions, $\beta = G\gamma'/(2\mu + 3\mu')R$, $\gamma' = \mathrm{d}\gamma/\mathrm{d}T$, μ is the viscosity of the dispersing liquid and $\mu' \sim \alpha_4$ is the viscosity of the cholesteric phase, supposed to behave as an isotropic liquid of viscosity α_4.

This calculation shows that the rotation velocity is proportional to G and is odd in q, which means that the droplets stop rotating when their director field is not twisted. The rotation velocity is also proportional to γ', the driving force for the Marangoni flow, and is inversely proportional to the viscosities, as expected intuitively and checked experimentally [18]. This formula also shows that ω and G are of opposite signs when $q > 0$ (right-handed cholesteric) and $\gamma' < 0$. This is well observed in experiments with the PF-656. Finally, this calculation shows that the rotation velocity crucially depends on the orientation of the helical axis. Indeed, the rotation
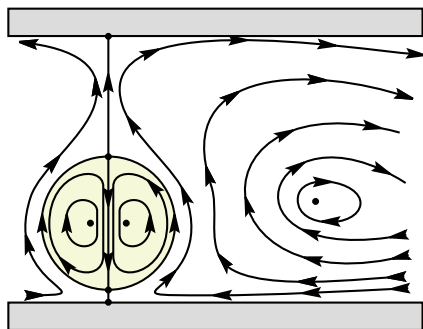
Figure 22. Schematic representation of the streamlines inside (Hill vortex in yellow) and outside of the droplet.

velocity exactly vanishes in this calculation when $\alpha = 0$ (helical axis parallel to $\bar{G}$) and is maximal when $\alpha = \pi/2$ corresponding to the banded droplets.[10] For these droplets, the predicted velocity is typically three times larger than that measured experimentally although the dependence on the radius is the same. This lack of quantitative agreement is not surprising given the approximations made on the director and velocity fields. Other director fields satisfying the homeotropic anchoring at the surface of the droplet have been tested in Ref. [18] and led to velocities comparable to those of the spiraling droplets. For this reason, we think that this model coupling the director field to the Marangoni flows is a good candidate to explain the Lehmann effect in emulsions.

However, this model certainly does not apply in the coexistence region, since it predicts that CC droplets do not rotate, in complete disagreement with experiments. In addition, there is, to the best of our knowledge, no experimental evidence that the surface tension is temperature dependent in the coexistence region.

5. Conclusion

This review shows that the Lehmann effect is a fascinating – but complex – phenomenon, still far from being fully understood although it was discovered almost 120 years ago. The experiments in the coexistence region and in emulsions suggest that many mechanisms could operate at the same time. At the current state of our knowledge, the model of melting-growth is very promising to explain the Lehmann effect in the coexistence region, while the Marangoni model rather applies in emulsions. By contrast, the thermomechanical explanation, first proposed by Leslie in 1968 and which became a paradigm, fails to explain the observations in all systems, both quantitatively and qualitatively. For this reason and to avoid confusion, we propose that the thermomechanical effect discovered by Leslie, and that was evidenced experimentally, will no longer be called the Lehmann effect, by reserving this term for the rotation of the twisted nematic and cholesteric droplets in a temperature gradient, whatever the mechanisms involved in the rotation process. This new definition of the Lehmann effect so embraces the own Lehmann experiments that were presumably performed with emulsified cholesterics, but also the more recent experiments performed with nematics and cholesterics in both the coexistence region and the partly miscible emulsions.

It is now clear that new experiments should be performed in the future to clarify the problem of the flows in the coexistence zone, in particular across the sample. It would also be interesting to reproduce the experiment of Nishiyama et al. [44] with the TB and CC droplets to test whether a particle attached to their surface rotates. According to these authors, the particle should not rotate as everybody agrees that these droplets do not rotate as rigid bodies. By contrast, our prediction is that the particle should rotate with the texture if our explanation in terms of anchoring force is correct. The experiment on the inverse Lehmann effect should also be reproduced because its order of magnitude, if confirmed experimentally, is amazing and would provide new challenges for theorists. It would also be important to develop new numerical techniques such as the one proposed in Refs. [29,47,54,95] to reconstruct the director field inside the droplets and compare numerically simulated optical micrographs with experimental ones. This would be crucial to test new theoretical models, as we know that the rotation velocity of the droplets strongly depends on their texture.

Notes

1. Note that because of the errors on the measurement of $C^\star$, a very slow rotation due to the Leslie effect as the one described in Ref. [81] cannot be excluded at this concentration.
2. Note that this mechanism does not depend on the polar or azimuthal nature of the anchoring: if we assume an easy axis p (which can be planar, homeotropic or tilted with respect to the surface) for the interaction energy between the cholesteric droplet and the particle, the particle will simply minimize this interaction energy by shifting its position to a point where $n = \pm p$ (the two signs are due to the symmetry $n \to -n$).
3. Note that the thermomechanical effects of Leslie, Akopyan and Zel'dovich are very much relevant in experiments performed below the transition temperature with fully cholesteric samples [28,33,34,76–78,81,96] or nematic samples with a deformed texture [83]. Such systems are

outside the scope of this paper, which only focus on the Lehmann rotation of cholesteric droplets.

4. In the original paper of Akopyan and Zel'dovich, the phenomenological equations do not respect Onsager reciprocity relations. This problem is addressed in the rigorous framework used by Pleiner and Brand to derive the same type of terms.

5. In principle, this torque can also contain viscous and thermomechanical contributions coming from the surfacic production of entropy, but these terms are generally neglected in cholesterics and nematics.

6. Indeed, in the Ericksen–Leslie theory the thermomechanical stress and torque of Leslie, Akopyan and Zel'dovich just appear as additional terms in the general expression of the internal viscous stress and torque. These terms proportional to the temperature gradient are allowed by symmetries only in pure cholesterics (Leslie terms) and in deformed nematics and cholesterics (Akopyan and Zel'dovich terms).

7. Note that this equation could also been obtained by applying the angular momentum theorem to a ball of radius R_b larger than R (the radius of the droplet) and by then making R_b tend to R.

8. Note that in this calculation we consider that f (or W) is an explicit function of T and the spatial coordinates: $f(T, r, \theta, z)$. For this reason $(\partial f/\partial T)(\partial T/\partial \theta)$ is in general different from $\partial f/\partial \theta$, the integral of which is equal to 0 as underlined by one of the reviewers. Indeed, let us suppose that $f(T, r, \theta, z) = Th(r, \theta, z)$. Then, $(\partial f/\partial T)(\partial T/\partial \theta) = h(\partial T/\partial \theta) \neq \partial f/\partial \theta = T(\partial h/\partial \theta) + h(\partial T/\partial \theta)$ (by assuming, this time, that f is a function of (r, θ, z) only).

9. This can be checked by noting that the rigorous (covariant) expression of $\partial T/\partial \theta$ is $(\vec{u} \times \vec{r}) \cdot \vec{\nabla} T$, where $\vec{u}$ is the polar axis and $\vec{r}$ is the spatial position. Since $(\vec{u} \times \vec{r})$ is a pseudo-vector (it changes sign under the mirror transformation) and $\vec{\nabla} T$ is a true vector (it stays invariant under the mirror transformation), $\partial T/\partial \theta$ changes its sign under the transformation $q \to -q$ (equivalent to a mirror transformation).

10. These results show that the droplets do not work as mechanical turbines at all, as might be intuitively thought.

Disclosure statement

No potential conflict of interest was reported by the authors.

References

[1] Chandrasekhar S. Hydrodynamic and hydromagnetic stability. New York: Dover; 1981.

[2] Ronsin O, Heslot F, Perrin B. Experimental study of quasistatic brittle crack propagation. Phys Rev Lett. 1995;75:2352–2355.

[3] Rittel D. Thermomechanical aspects of dynamic crack initiation. Int J Fract. 1999;99:199–209.

[4] Soumahoro Z, Maigre H. Thermomechanical coupling dynamic crack propagation. Universal J Frac Mech. 2016;4:70–85.

[5] London H. Thermodynamics of the thermomechanical effect of liquid He II. Proc R Soc Lond A. 1939;171:484–496.

[6] Yariv E, Brenner H. Flow animation by unsteady temperature fields. Phys Fluids. 2004;16:L95–L98.

[7] Kataoka DE, Troian SM. Patterning liquid flow on the microscopic scale. Nature. 1999;402:L95–L98.

[8] Weinert FM, Braun D. Optically driven fluid flow along arbitrary microscale patterns using thermoviscous expansion. J Appl Phys. 2008;104:104701.

[9] Kim YK, Senyuk B, Lavrentovich OD. Molecular reorientation of a nematic liquid crystal by thermal expansion. Nat Commun. 2012;3:1133.

[10] Lehmann O. Structur, System und magnetisches Verhalten flüssiger Krystalle und deren Mischbarkeit mit festen. Ann Phys. 1900;307:649–705.

[11] Kottas GS, Clarke LI, Horinek D, et al. Artificial molecular rotors. Chem Rev. 2005;105:1281–1376.

[12] Michl J, Sykes ECH. Molecular rotors and motors: recent advances and future challenges. ACS Nano. 2009 May;3:1042–1048.

[13] Lehmann O. Flüssige Krystalle und ihr scheinbares Leben. Leipzig: Verlag von Leopold Voss; 1921.

[14] Oseen CW. The theory of liquid crystals. Trans Far Soc. 1933;29:883–899.

[15] Leslie FM. Some thermal effects in cholesteric liquid crystals. Proc R Soc A. 1968;307(1490):359–372.

[16] Oswald P, Dequidt A. Measurement of the continuous Lehmann rotation of cholesteric droplets subjected to a temperature gradient. Phys Rev Lett. 2008;100:217802.

[17] Yoshioka J, Araoka F. Topology-dependent self-structure mediation and efficient energy conversion in heat-flux-driven rotors of cholesteric droplets. Nat Commun. 2018;9:432.

[18] Oswald P, Ignés-Mullol J, Dequidt A. Lehmann rotation of cholesteric droplets driven by Marangoni convection. Soft Matter. 2019;15:2591–2604.

[19] Hanson H, Dekker AJ, van der Woude F. Analysis of the pitch in binary cholesteric liquid crystal mixtures. J Chem Phys. 1975;62:1941–1946.

[20] Oswald P, Dequidt A, Żywociński A. Sliding planar anchoring and viscous surface torque in a cholesteric liquid crystal. Phys Rev E. 2008;77:061703.

[21] Yoshioka J, Ito F, Suzuki Y, et al. Director/barycentric rotation in cholesteric droplets under temperature gradient. Soft Matter. 2014;10:5869.

[22] Ito F, Yoshioka J, Tabe Y. Heat-driven rotation in cholesteric droplets with a double twisted structure. J Phys Soc Japan. 2016;85:114601.

[23] Yoshioka J, Ito F, Tabe Y. Stability of a double twisted structure in spherical cholesteric droplets. Soft Matter. 2016;12:2400–2407.

[24] Yamamoto T, Kuroda M, Sano M. Three-dimensional analysis of thermo-mechanically rotating cholesteric liquid crystal droplets under a temperature gradient. Europhys Lett. 2015;109:46001.

[25] Kahn FJ, Taylor GN, Schonhorn H. Surface-produced alignment of liquid crystals. Proc IEEE. 1973;61:823–828.

[26] Bono S, Sato S, Tabe Y. Unidirectional rotation of cholesteric droplets driven by UV-light irradiation. Soft Matter. 2017;13:6569–6575.

[27] Faetti S, Palleschi V. Nematic-isotropic interface of some members of the homologous series of 4-cyano-4′-(n-alkyl)biphenyl liquid crystals. Phys Rev A. 1984;30:3241–3251.

[28] Oswald P, Poy G, Dequidt A. Lehmann rotation of twisted bipolar cholesteric droplets: role of Leslie, Akopyan and Zeľdovich thermomechanical coupling terms of nemato-dynamics. Liq Cryst. 2017;44:969–988.

[29] Poy G, Bunel F, Oswald P. Role of anchoring energy on the texture of cholesteric droplets: finite-element simulations and experiments. Phys Rev E. 2017;96:012705.

[30] Oswald P. Microscopic vs. macroscopic origin of the Lehmann effect in cholesteric liquid crystals. Eur Phys J E. 2012;35:10.

[31] Krimer OD, Residori S. Thermomechanical effects in uniformly aligned dye-doped nematic liquid crystals. Eur Phys J E. 2007;23:77–82.

[32] Aleksanyan AK, Minasyan AK, Hakobyan RS. Convective motions in nematic liquid crystal homeotropic and planar cells induced by Gaussian laser beam. Int J Mod Phys: Conf Series. 2011;15:129–139.

[33] Dequidt A. Effet Lehmann dans les cristaux liquides cholestériques [dissertation]. Université de Lyon, Ecole Normale Supérieure de Lyon; 2008.

[34] Poy G. Sur la pertinence du modèle thermomécanique dans la rotation Lehmann des gouttes cholestériques et nématiques [dissertation]. Université de Lyon, Ecole Normale Supérieure de Lyon; 2017.

[35] Oswald P. Lehmann rotation of cholesteric droplets subjected to a temperature gradient: role of the concentration of chiral molecules. Eur Phys J E. 2009;28:377–383.

[36] Oswald P, Jørgensen L, Żywociński A. Lehmann rotatory power: a new concept in cholesteric liquid crystals. Liq Cryst. 2011;38:601–613.

[37] Oswald P, Pirkl S. Lehmann rotation of the cholesteric helix in droplets oriented by an electric field. Phys Rev E. 2014;89:022509.

[38] Oswald P, Poy G. Lehmann rotation of cholesteric droplets: role of the sample thickness and of the concentration of chiral molecules. Phys Rev E. 2015;91:032502.

[39] Oswald P, Pieranski P. Nematics and cholesteric liquid crystals: concepts and physical properties illustrated by experiments. Boca Raton: Taylor & Francis; 2005.

[40] Bono S, Maruyama Y, Tabe Y. Formation and dynamics of the aggregates of cholesteric double-twist cylinders. Soft Matter. 2018;14(48):9798–9805.

[41] Bono S, Maruyama Y, Nishiyama K, et al. A thermomechanical coupling in cholesteric liquid crystals: unidirectional rotation of double-twist cylinders driven by heat flux. Eur Phys J E. 2019;42:99.

[42] Bono S, Maruyama Y, Nishiyama K, et al. Photocontrollable rotation of cholesteric double-twist cylinders. Mol Cryst Liq Cryst. 2019;683:39–45.

[43] Poy G, Oswald P. Do Lehmann cholesteric droplets subjected to a temperature gradient rotate as rigid bodies? Soft Matter. 2016;12:2604–2611.

[44] Nishiyama K, Bono S, Maruyama Y, et al. Direct observation of rigid-body rotation of cholesteric droplets subjected to a temperature gradient. J Phys Soc Jpn. 2019;88:063601.

[45] Madhusudana NV, Pratibha R. Elasticity and orientational order in some cyanobiphenyls: Part IV. Reanalysis of the data. Mol Cryst Liq Cryst. 1982;89(1-4):249–257.

[46] Valignat MP, Villette S, Li J, et al. Wetting and anchoring of a nematic liquid crystal on a rough surface. Phys Rev Lett. 1996;77(10):1994–1997.

[47] Ravnik M, Žumer S. Landau–de Gennes modelling of nematic liquid crystal colloids. Liq Cryst. 2009;36:1201–1214.

[48] Kitahata H. Rigid-body rotation or director rotation? the direct observation gave the answer to the question. JPSJ News Comments. 2019;16:10.

[49] Kozbial A, Guan W, Li L. Manipulating the molecular conformation of a nanometer-thick environmentally friendly coating to control the surface energy. J Mater Chem A. 2017;5:9752–9759.

[50] Finkenzeller U, Geelhaar T, Weber G, et al. Liquid-crystalline reference compounds. Liq Cryst. 1989;5:313–321.

[51] Oswald P, Poy G. Role of impurities in the Lehmann effect of cholesteric liquid crystals: towards an alternative model. Phys Rev E. 2018;98:032704.

[52] Seč D, Porenta T, Ravnik M, et al. Geometrical frustration of chiral ordering in cholesteric droplets. Soft Matter. 2012;8:11982–11988.

[53] Seč D, Čopar S, Žumer S. Topological zoo of free-standing knots in confined chiral nematic fluids. Nat Commun. 2014;5:3057.

[54] Posnjak G, Čopar S, Muševic I. Hidden topological constellations and polyvalent charges in chiral nematic droplets. Nat Commun. 2017;8:14594.

[55] Krakhalev MN, Gardymova AP, Prishchepa OO, et al. Bipolar configuration with twisted loop defect in chiral nematic droplets under homeotropic surface anchoring. Sci Rep. 2017;7:14582.

[56] Yoshioka J, Fukao K. Horizontal transportation of a maltese cross pattern in nematic liquid crystalline droplets under a temperature gradient. Phys Rev E. 2019;99:022702.

[57] Yamamoto T, Sano M. Hydrodynamic Rotlet dipole driven by spinning chiral liquid crystal droplets. Phys Rev E. 2019;99:022704.

[58] Allen C, Wu TYT. Hydromechanics of low-Reynolds-number flow. Part 2. Singularity method for stokes flows. J Fluid Mech. 1975;67(4):787–815.

[59] Jeong J, Davidson ZS, Collings PJ, et al. Chiral symmetry breaking and surface faceting in chromonic liquid crystal droplets with giant elastic anisotropy. Proc Natl Acad Sci. 2014;111(5):1742–1747.

[60] Volovik GE, Lavrentovich OD. Topological dynamics of defects: Boojums in nematic drops. Zh Eksp Teor Fiz. 1983;85(6):1997–2010.

[61] Williams RD. Two transitions in tangentially anchored nematic droplets. J Phys A: Math Gen. 1986;19:3211–3222.

[62] Lavrentovich OD, Sergan VV. Parity-breaking phase transition in tangentially anchored nematic drops. Il Nuovo Cimento D. 1990;12:1219–1222.

[63] Zhou S, Nastishin YA, Omelchenko MM, et al. Elasticity of lyotropic chromonic liquid crystals probed by director reorientation in a magnetic field. Phys Rev Lett. 2012;109:037801.

[64] Ignés-Mullol J, Poy G, Oswald P. Continuous rotation of achiral nematic liquid crystal droplets driven by heat flux. Phys Rev Lett. 2016;117:057801.

[65] Sato S, Bono S, Tabe Y. Unidirectional heat transport driven by rotating cholesteric droplets. J Phys Soc Japan. 2017;86:023601.

[66] Svenšek D, Pleiner H, Brand HR. Inverse Lehmann effects can be used as a microscopic pump. Phys Rev E. 2008;78:021703.

[67] Akopyan RS, Zeldovich BY. Thermomechanical effects in deformed nematics. JETP. 1984;87:1660–1669.

[68] Pleiner H, Brand HR. Hydrodynamics and electrohydrodynamics of liquid crystals. In: Buka A, Kramer L, editors. Pattern formation in liquid crystals. NY; Springer; 1996. p. 15–69.

[69] Sarman S. Molecular dynamics simulation of thermomechanical coupling in cholesteric liquid crystals. Mol Phys. 2000;98:27–35.

[70] Sarman S. Transport properties of cholesteric liquid crystals studied by molecular dynamics simulation. Mol Phys. 2001;99:1235–1247.

[71] Sarman S, Laaksonen A. Thermomechanical coupling, heat conduction and director rotation in cholesteric liquid crystals studied by molecular dynamics simulations. Phys Chem Chem Phys. 2012;15:1235–1247.

[72] Dequidt A, Poy G, Oswald P. Generalized drift velocity of a cholesteric texture in a temperature gradient. Soft Matter. 2016;12:7529–7538.

[73] de Gennes PG, Prost J. The physics of liquid crystals. Oxford: Oxford University Press; 1993.

[74] Leslie FM. Thermo-mechanical coupling in cholesteric liquid crystals. Symp Faraday Soc. 1971;5:33–40.

[75] Poy G, Oswald P. On the existence of the thermomechanical terms of Akopyan and Zeľdovich in cholesteric liquid crystals. Liq Cryst. 2018;45:1428–1442.

[76] Éber N, Jánossy I. An experiment on the thermomechanical coupling in cholesterics. Mol Cryst Liq Cryst. 1982 Jan;72:233–238.

[77] Éber N, Jánossy I. Thermomechanical coupling in compensated cholesterics. Mol Cryst Liq Cryst. 1984;102: 311–316.

[78] Dequidt A, Żywociński A, Oswald P. Lehmann effect in a compensated cholesteric liquid crystal: experimental evidence with fixed and gliding boundary conditions. Eur Phys J E. 2008;25:277–289.

[79] Oswald P. Leslie thermomechanical power in diluted cholesteric liquid crystals. Europhys Lett. 2014 Nov;108: 36001.

[80] Oswald P. Erratum: Leslie thermomechanical power in diluted cholesteric liquid crystals. Europhys Lett. 2014;108:59901.

[81] Oswald P, Dequidt A. Direct measurement of the thermomechanical Lehmann coefficient in a compensated cholesteric liquid crystal. Europhys Lett. 2008;83:16005.

[82] Oswald P. About the Leslie explanation of the Lehmann effect in cholesteric liquid crystals. Europhys Lett. 2012;97:36006.

[83] Akopyan RS, Alaverdian RB, Santrosian EA, et al. Thermomechanical effects in the nematic liquid crystals. J Appl Phys. 2001;90:3371–3376.

[84] Manzo C, Paparo D, Marrucci L, et al. Light-induced rotation of dye-doped liquid crystal droplets. Phys Rev E. 2006;73:051707.

[85] Oswald P, Poy G. Droplet relaxation in Hele-Shaw geometry: application to the measurement of the nematicisotropic surface tension. Phys Rev E. 2015;92: 062512.

[86] Dunmur DA, Miller WH. Volumetric studies of the homologous series of alkyl-cyano-biphenyl liquid crystals. J Phys Paris. 1979;40(C3):141–146.

[87] Fournier JB. Generalized Gibbs–Thomson equation and surface stiffness for materials with an orientational order parameter. Phys Rev Lett. 1995;75:854–857.

[88] Gray GW, Harrison KJ, Nash JA. New family of nematic liquid crystals for displays. Electron Lett. 1973;9: 130.

[89] Tabe Y, Yokoyama H. Coherent collective precession of molecular rotors with chiral propellers. Nat Mater. 2003;2:806–809.

[90] Milczarczyk-Piwowarczyk P, Żywociński A, Noworyta K, et al. Collective rotations of ferroelectric liquid crystals at the air/water interface. Langmuir. 2008;24:12354–12363.

[91] Bunel F, Ignés-Mullol J, Saguès F, et al. Chemical Leslie effect in Langmuir monolayers: a complete experimental characterization. Soft Matter. 2018;14:4835–4845.

[92] Seki K, Ueda K, Okumura YI, et al. Non-equilibrium dynamics of 2D liquid crystals driven by transmembrane gas flow. J Phys: Condens Matter. 2011;23:284114.

[93] Darmon A, Benzaquen M, Čopar S, et al. Topological defects in cholesteric liquid crystal shells. Soft Matter. 2016;12:9259–9392.

[94] Young NO, Goldstein JS, Block MJ. The motion of bubbles in a vertical temperature gradient. J Fluid Mech. 1959;6:350–356.

[95] Poy G, Žumer S. Ray-based optical visualisation of complex birefringent structures including energy transport. Soft Matter. 2019;15:3659–3670.

[96] Dequidt A, Oswald P. Lehmann effect in compensated cholesteric liquid crystals. Europhys Lett. 2007;80: 26001.